2016-09-01

An Exploration in Fiber Optic Sensors

Frederick Alexander Seng
Brigham Young University

An Exploration in Fiber Optic Sensors

Frederick Alexander Seng

A thesis submitted to the faculty of
Brigham Young University
in partial fulfillment of the requirements for the degree of

Master of Science

Stephen Schultz, Chair
Aaron Hawkins
Gregory Nordin

Department of Electrical and Computer Engineering

Brigham Young University

2016

ABSTRACT

An Exploration in Fiber Optic Sensors

Frederick Alexander Seng
Department of Electrical and Computer Engineering, BYU
Master of Science

With the rise of modern infrastructure and systems, testing and evaluation of specific components such as structural health monitoring is becoming increasingly important. Fiber optic sensors are ideal for testing and evaluating these systems due many advantages such as their lightweight, compact, and dielectric nature. This thesis presents a novel method for detecting electric fields in harsh environments with slab coupled optical sensors (SCOS) as well as a novel method for detecting strain gradients on a Hopkinson bar specimen using fiber Bragg gratings (FBG).

Fiber optic electric field sensors are ideal for characterizing the electric field in many different systems. Unfortunately many of these systems such as railguns or plasma discharge systems produce one or more noise types such as vibrational noise that contribute to a harsh environment on the fiber optic sensor. When fiber optic sensors are placed in a harsh environment, multiple noise types can overwhelm the measurement from the fiber optic sensor. To make the fiber optic sensor suitable for a harsh environment it must be able to overcome all these noise types simultaneously to operate in a harsh environment rather than just overcome a single noise type. This work shows how to eliminate three different noise types in a fiber optic sensor induced by a harsh environment simultaneously. Specifically, non-localized vibration induced interferometric noise is up converted to higher frequency bands by single tone phase modulation. Then localized vibrational noise, and radio frequency (RF) noise are all eliminated using a push-pull SCOS configuration to allow for an optical measurement of an electric field in a harsh environment.

The development and validation of a high-speed, full-spectrum measurement technique is described for fiber Bragg grating sensors in this work. A fiber Bragg grating is surface mounted to a split Hopkinson tensile bar specimen to induce high strain rates. The high strain gradients and large strains which indicate material failure are analyzed under high strain rates up to 500 s^{-1}. The fiber Bragg grating is interrogated using a high-speed full-spectrum solid state interrogator with a repetition rate of 100 kHz. The captured deformed spectra are analyzed for strain gradients using a default interior point algorithm in combination with the modified transfer matrix approach. This work shows that by using high-speed full-spectrum interrogation of a fiber Bragg grating and the modified transfer matrix method, highly localized strain gradients and discontinuities can be measured without a direct line of sight.

Keywords: Fiber Optics, SCOS, Electric Field Sensing,

ACKNOWLEDGEMENTS

I would first like to thank Dr. Stephen Schultz for this opportunity. He has been a great mentor and friend, and has taught me how to analyze critical problems on my own. I would like to thank my mentors: Spencer Chadderdon who taught me to push myself to grow in research, and Nikola Stan, for all his love and support and positive attitude. I could not have done this without you.

I would like to thank my family. To my dear wife Wendy, thank you for staying with me and believing in us. Thank you for taking care of our children for 4 years so that I could complete my bachelor studies. I would not be an engineer today if it was not for your love and support. I look forward to raising our children, I love you more than anything in the world, I look forward to spending eternity with you.

Thank you to my parents who have always supported me in terms of finance and love. Thank you to my in-laws for helping make time for Wendy and I in our pursuits, to my mother in law, who gave me the opportunity to grow when I was in need. Thank you to my grandparents who taught me how to work, my uncle who taught me how to think.

Thank you to Dr. Selfridge who always gave me encouragement, and thank you to the rest of the lab members who have been with me through this journey, Rex King, LeGrand Shumway, Alec Hammond, Chad Josephson, Alexander Petrie, Reid Worthen, Jessica Johnston, Ivann Velasco, and Helaman Johnston.

I would like to thank the Test Resource Management Center Test and Evaluation/Science and Technology Program for their financial support. This work is funded through U.S. Army Program Executive Office for Simulation, Training and Instrumentation.

TABLE OF CONTENTS

LIST OF FIGURES

1 INTRODUCTION

1.1 Fiber Optic Sensors

With the rise of modern infrastructure and systems, testing and evaluation of specific components such as structural health monitoring is becoming more and more important. High voltage systems are a good example of modern systems that need to be tested. In the hundreds of kilovolts range, testing becomes dangerous for traditional conductive test equipment as well as the people testing the system. However, through the use of fiber optic electric field sensors, this problem can be mitigated drastically. Fiber optic sensors are ideal for these applications due to numerous advantages such as their compact, dielectric and lightweight nature.

Figure 1-1 shows a commercially available electric field sensor called the D-dot, which is very sensitive. But its large physical size and metallic nature disrupts the fields being measured. Testing of systems that have tighter spaces does not allow for the use of this sensor. Figure 1-2 shows a fiber optic variant of the D-dot called a slab coupled optical sensor (SCOS). The SCOS has a sensing region of 1 mm parallel to the direction of the fiber and 0.3 mm perpendicular to the length of the fiber, allowing it to fit into very tight spaces.

Despite numerous advantages over their semiconductor/metal counterparts, fiber optic sensors still have a considerable amount of research that needs to be performed to improve performance and applicability. For example, fiber optic sensors in general aren't as sensitive as

their metal counterparts. This work focuses on making two types of fiber optic sensors more applicable to real world applications.

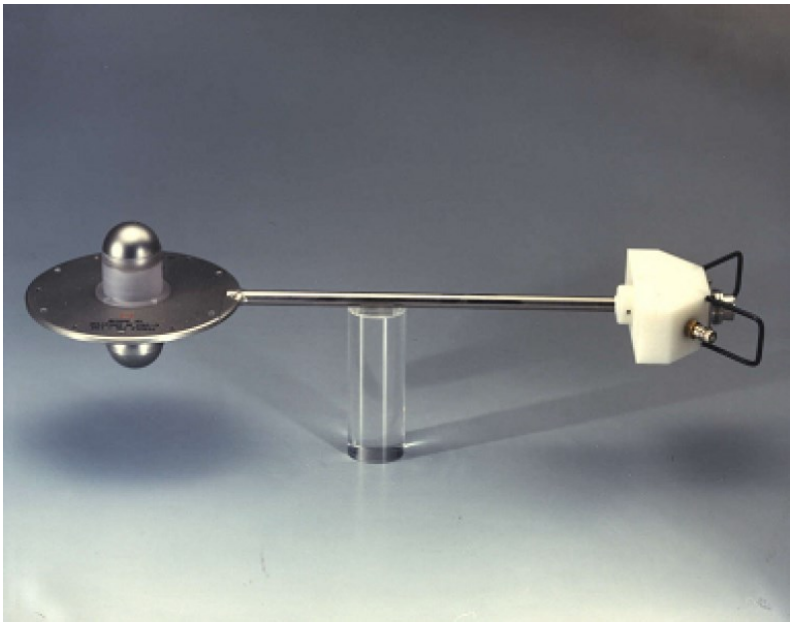

Figure 1-1: Commercially available D-dot sensor.

Figure 1-2: The slab coupled optical sensor (SCOS) has a measurement cross section of 1 mm along the length of the fiber and 0.3 mm perpendicular to the length of the fiber.

The first sensor this work focuses on is the electric field fiber optic sensor called a slab coupled optical sensor (SCOS) under operation in a harsh environment. A new differential push-pull variant of the SCOS is made to subtract out noise, and when coupled with phase modulation

to reduce interferometric noise, it is possible for the SCOS to measure electric fields in a harsh environment. In other words, this thesis shows a method to take out three different noise types in a SCOS simultaneously to handle a harsh environment.

The second sensor this work focuses on is a strain/temperature fiber optic sensor, the fiber Bragg grating (FBG). Previous work done at BYU on making the FBG more applicable to real world applications involved developing a high-speed full-spectrum interrogator for the FBG. This work validates the novel high-speed full-spectrum interrogation technique for FBGs through the measurement of an FBG on a Hopkinson bar. This allows for strain gradients and indications of damage failure in a Hopkinson bar specimen or any specimen under a dynamic test to be analyzed without a direct line of sight.

1.2 Optical Sensing of Electric Field in Harsh Environments

The performance of many systems can be characterized by measuring the electric field they produce under operation. The compact dielectric nature of fiber optic electric field sensors are ideal for measuring the electric field signals of these systems[1][2][3]. Unfortunately, many of these systems also produce multiple noise types which contribute to a harsh environment and can drown out the electric field measurement obtained by fiber optic sensor [4]. In order to overcome this harsh environment the fiber optic sensor must be able to simultaneously overcome all the different noise types from a system.

Figure 1-3 shows that examples of systems that need to have their electric field characterized and produce harsh environments on fiber optic electric field sensors are rail guns that produce huge amounts of vibrational and acoustic noise under operation [5][6], and plasma

discharge systems for combustion ignition which produce a significant amount of vibrational and RF noise [7][8].

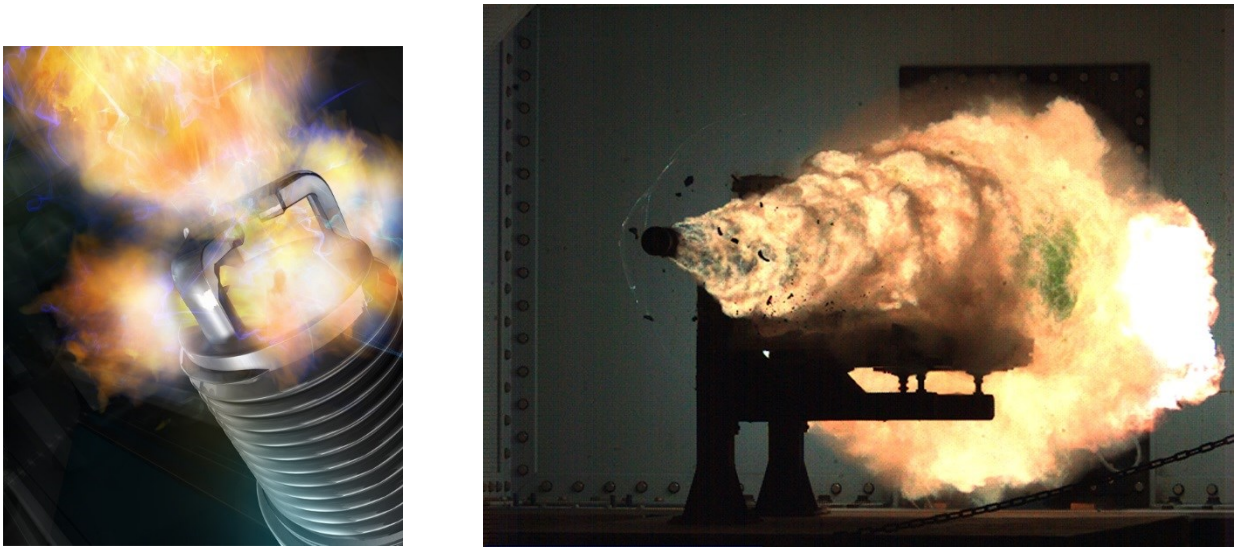

Figure 1-3 a) Spark plugs and b) railguns are examples of systems that produce large amounts of vibration and thermal noise under operation.

Fiber optic sensor requirements in harsh environments are plenty, different systems are different harsh environments, and different harsh environments produce different noise types. Some environments produce thermal noise [9], some produce large vibrations [10] , and some produce both [11].

The most important characteristic of a fiber optic sensor suited for a harsh environment is getting rid of the different noise types simultaneously. In other words, it must be able to overcome a harsh environment rather than just simply overcome a noise source.

This work shows the application for slab coupled optical sensors (SCOS) [1][12] for sensing electric fields in harsh environments. The three noise types the harsh environment in this work produces are localized vibration noise on the sensing element, non-localized vibration

noise induced on any segment of the fiber connected to the sensor, and finally radio frequency (RF) noise induced on the electronic interrogation system.

Non-localized vibration which manifests itself as interferometric noise is first eliminated by up converting and filtering out the noise using single tone phase modulation, then localized vibration noise and RF noise are eliminated through the push-pull SCOS configuration. By eliminating all three noise sources simultaneously, fiber optic sensing of electric fields in a harsh environment can be achieved. In other words, the SCOS is capable of overcoming a harsh environment rather than a noise source.

1.3 Split Hopkinson Bar Measurements using FBGs

Full field measurement techniques such as Digital Image Correlation (DIC) are often used to capture the dynamic deformation of materials. However, these methods require a direct line of sight as they rely on optical imaging, for which many applications are not conducive.

Fiber Bragg gratings (FBGs) are a promising tool to test a variety of different material systems at high strain rates due to their sensitivity and response time, and ability to be surface mounted or embedded in samples. There have been previous studies where the FBG was embedded in a composite split Hopkinson tensile bar specimen such as polymer reinforced carbon fiber, and peak tracking was used to measure the average strain under high strain rate conditions. It has been shown that FBGs offer better sensitivity and quicker response times than traditional electrical strain gauges which are often used to interrogate a Hopkinson bar [13][14][15].

It has been shown that the spatial resolution of FBGs can be increased by measuring the strain distribution along the FBG [16][17]. This is particularly useful for measuring strain

gradients and profiles along a material, which are generally the initiations of damage localization such as cracks or plastic deformations [18].

However, deducing the strain profile along an FBG requires capturing the spectrum of the FBG which contains the information about the distributed strain. This becomes difficult at high strain rates where a high-speed full-spectrum FBG interrogator is required [19].

A well-known method for testing material behavior at high strain rates is through a split Hopkinson tensile bar [20][21], which is capable of generating high compressive, tensile, or torsional strain rates well above $10^2 s^{-1}$[22]. Due to these high strain rates, a low data acquisition rate can result in the loss of important data. It has been shown in research findings that the successful use of a split Hopkinson bar requires the components in the data acquisition system to have a minimum frequency response of at least 100 kHz [23][24].

Hopkinson bar testing is difficult especially in tension because the whole specimen may not be in equilibrium and different parts of the specimen strain different amounts due to the geometry of the specimen. By monitoring the progression of these strain waves, the mechanical response (stress vs strain) along with ultimate strength of the specimen can be understood as a function of strain rate along with information about localization that may occur during failure [25][26]. As a result, methods such as DIC have been used to interrogate the specimen of the Hopkinson bar because the strain profile is not necessarily constant along the length of the specimen. However, full view of the specimen is not always available; therefore strain gauges are often required.

This work shows that through high-speed full-spectrum interrogation of FBGs, distributed strain and strain gradients along the surface of a Hopkinson bar specimen can be captured using

an FBG up to 500 s^{-1}. By using this method, FBG spectrum distortions which contain information about high speed distributed strain can be captured and analyzed. This allows for strain gradients and initial signs of failure in the material to be identified.

The novel contribution of this work is that by using high-speed full-spectrum interrogation of a fiber Bragg grating and the modified transfer matrix method, highly localized strain gradients and discontinuities can be measured without a direct line of sight. An FBG surface mounted on a Hopkinson bar specimen was used to validate the new high-speed method by verifying the strain along the length of a specimen at high rates. For this experiment, the FBG strain measurements were performed at a visible location so that they could be independently verified through DIC.

1.4 Contributions and Thesis Outline

This thesis consists of two main parts. The first part discusses harsh environment sensing using SCOS technology, including the operation and fabrication of a push-pull SCOS, interferometric noise reduction, and RF noise reduction. This information is presented in Chapter 2. The second part focuses on my major contributions towards high-speed full-spectrum interrogation of an FBG and is presented in Chapter 3. My major contributions deal with sensing of electric fields in harsh environments using SCOS and high-speed full-spectrum interrogation of FBGs. My major contributions are presented as follows:

1. I developed an interrogation method to reduce 3 separate noise sources simultaneously in a SCOS in a harsh environment.

(F. Seng, N. Stan, R. King, C. Josephson, L. Shumway, A. Hammond, and S. Schultz. "Optical sensing of Electric Fields in Harsh Environments." *Journal of Lightwave Technology,* under review.)

2. I developed a new SCOS prototype which is capable of handling localized vibration noise

   (F. Seng, N. Stan, C. Josephson, R. King, L. Shumway, R. Selfridge, S. Schultz. "Push-pull slab coupled optical sensor for measuring electric fields in a vibrational environment." Applied Optics 54.16 (2015): 5203-09.)

3. I developed a high-speed full-spectrum interrogation system and used it on a Hopkinson bar impact.

   (F. Seng, D. Hackney, T. Goode, L. Shumway, A. Hammond, G. Shoemaker, M. Pankow, K. Peters, and S. Schultz. "Split-Hopkinson Bar Measurement Using High-Speed Full-Spectrum Fiber Bragg Grating Interrogation." *Applied Optics,* Accepted.)

2 OPTICAL SENSING OF ELECTRIC FIELDS IN HARSH ENVIRONMENTS

The three noise sources stated in the introduction plague the slab coupled optical sensor (SCOS) and numerous other fiber optic sensors. To understand how the noise sources affect the SCOS its operation must first be understood.

2.1 The Slab Coupled Optical Sensor Background

Figure 2-1 shows that the SCOS consists of a lithium niobate crystal adhered to a polarization maintaining D-shaped optical fiber. It is crucial that the D-fiber is polarization maintaining since the sensitivity of the SCOS depends on interrogating the index change in the lithium niobate crystal through the r_{33} electro optic coefficient.

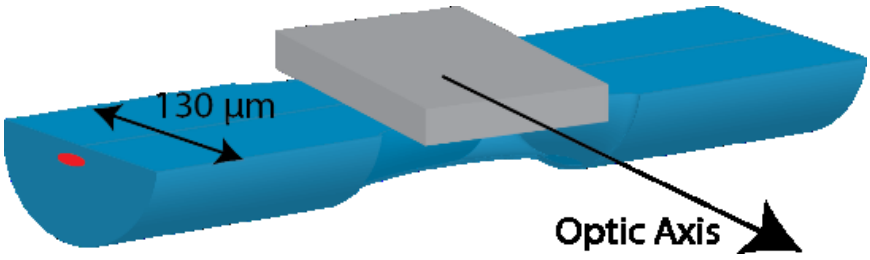

Figure 2-1: The slab coupled optical sensor (SCOS) consists of a lithium niobate crystal adhered to a D-shaped optical fiber.

The D-shaped optical fiber has a section where its flat region is etched down close to the elliptical polarization maintaining core via hydrofluoric acid for better coupling between the crystal and the fiber.

When the crystal is adhered onto the fiber, specific wavelengths of transverse polarized light in the direction of the lithium niobate optic axis can couple out of the fiber into the crystal as given by [1]

$$\lambda_m = \frac{2t}{m}\sqrt{n_o^2 - N_f^2}\,, \tag{2-1}$$

where t is the thickness of the slab waveguide, n_o is the refractive index of the slab waveguide, N_f is the effective index of the fiber mode, and m is the slab waveguide mode number.

Figure 2-2 shows that when certain wavelengths of light are coupled out of the D-fiber, that resonance dips form in the transmission spectrum of the optical fiber located at λ_m. When an electric field is applied in the direction of the optic axis of the lithium niobate crystal, the refractive index of the slab waveguide changes with respect to the r_{33} coefficient.

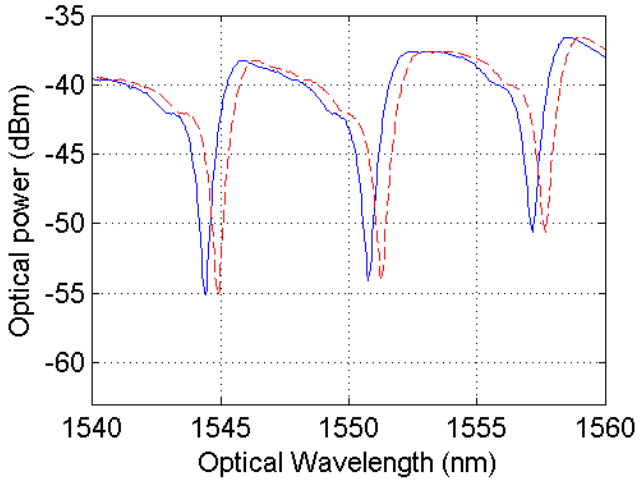

Figure 2-2: [27] Transmission spectrum of the SCOS (solid) without and (dashed) with an applied electric field

Equation (2-1) states that due to a change in the refractive index of the lithium niobate crystal the resonance dips shift from their original position to a new position. This shift will modulate the power of a laser with a wavelength onto a resonance edge launched into the D-fiber. By monitoring the change in power transmitted through the fiber, the electric field applied across the optic axis of the lithium niobate crystal can be deduced. The change in index in the lithium niobate crystal n_o with applied electric field is given by

$$\Delta n = n_o - \frac{1}{2} n_o^3 r_{33} E_z, \tag{2- 2}$$

where r_{33} is the linear electro-optic coefficient and E_z is the electric field in the transverse electric (TE) optic axis direction.

Unfortunately, Equation (2- **2**) also states that any random changes to N_f can also lead to a shift in the resonance. Changes to N_f are due to strain on the fiber and are considered to be localized vibration noise. This localized vibration noise and RF noise can be reduced by using the push-pull SCOS [27].

2.2 Localized Vibrational Noise Reduction Method Using the Push-Pull SCOS

In this work, two measurements are taken simultaneously from two different crystals. Figure 2-3 shows that the calibration factor for one of the channels is determined by measuring the transmitted signal while applying a known electric field resulting in

$$E_{m1} = 0.56 \frac{kV/m}{mV} V_m, \tag{2-3}$$

where V_m is the measured voltage and E_m is the corresponding measured electric field.

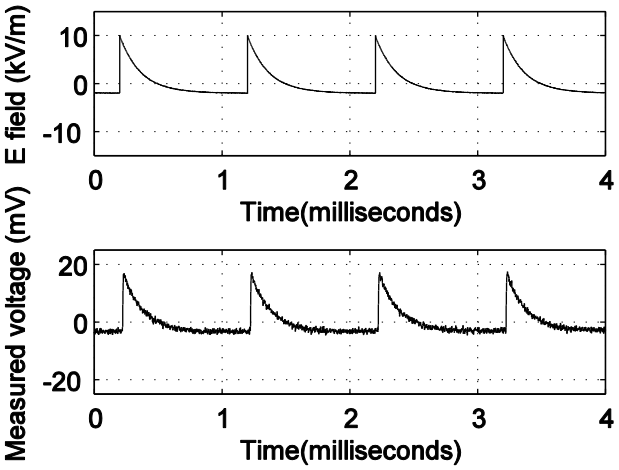

Figure 2-3: (top) Applied electric field and (bottom) measured voltage

The calibration factor for the other channel is determined in a similar manner and comes out to be

$$E_{m2} = 2.8\frac{kV/m}{mV}V_m . \tag{2-4}$$

Equation (2-1) shows that a change in the effective index of the fiber mode N_f also causes a shift in the transmission spectrum. This means that tensile as well as compressive stresses on the optical fiber cause a noticeable shift in the spectrum making the SCOS sensitive to vibrations.

Figure 2-4 shows the measured SCOS signal with an impact next to the SCOS. The sensitivity of the SCOS strain is estimated to be around 0.5 mV/microstrain. The impact causes a maximum strain of around 80 microstrain resulting in a noise voltage with a magnitude of around 40 mV, which is almost 4 times larger than the electric field induced signal shown in Figure 2-3. The strain induced signal can also be created through acoustic noise with no physical connection between the impact and the SCOS packaging [28].

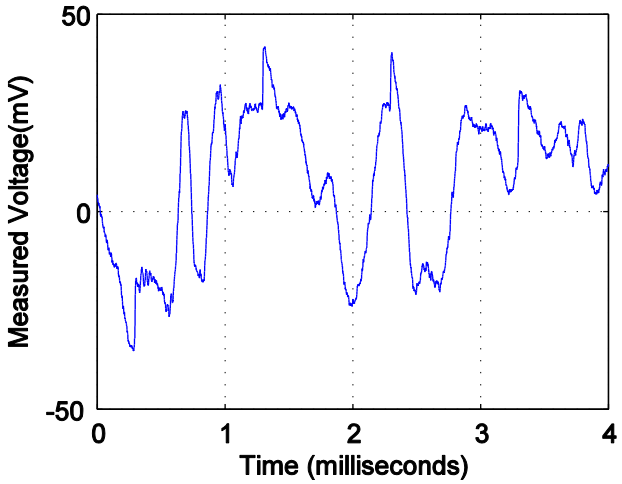

Figure 2-4: SCOS signal measured with an impact next to the SCOS.

In order to measure an electric field using the SCOS within a high vibration environment the SCOS signal either needs to be isolated from the vibration or the stress induced noise needs to be taken out of the measurement. In this work the stress induced signal is subtracted by attaching two crystals to the same D-fiber with opposing optic c axes of the crystal lattice.

2.3 Push-Pull Sensor Overview

Equation (2- **2**) shows that the change in the index of refraction is directly proportional to the electric field in the direction of the optic axis. This means that if an electric field is applied in the optic axis direction then the refractive index increases. If the crystal is then flipped 180 degrees without changing the electric field then the refractive index decreases. The sensor used in this work takes advantage of this directionality. The use of the directionality of nonlinear optical crystals has been used in electro-optic modulators [29][30] and is called a push-pull modulator because the applied voltage increases the refractive index in one arm of the modulator and reduces the refractive index in the other arm.

Figure 2-5 shows that the push-pull SCOS has 2 lithium niobate crystals coupled to a single D-fiber with their optic axes flipped opposite to each other. When an electric field is applied the refractive index of one crystal increases while that of the other crystal decreases. The result is that the transmission spectrum of one SCOS shifts towards higher wavelengths while the spectrum associated with the other SCOS shifts towards lower wavelengths.

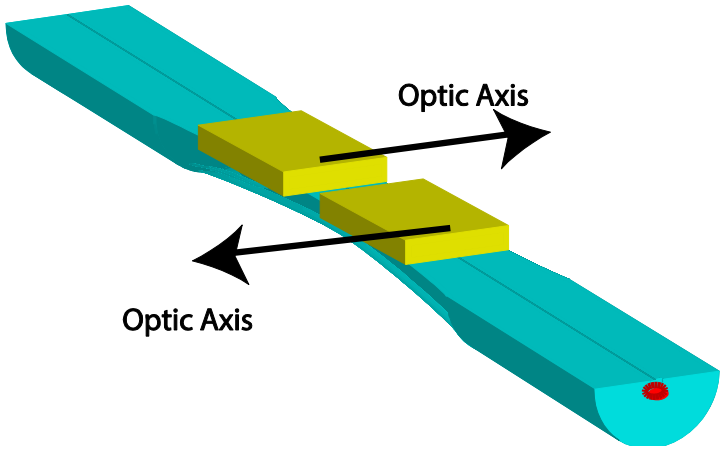

Figure 2-5: A push-pull SCOS consists of 2 lithium niobate crystals on a single D fiber with their optic axis flipped opposite with respect to each other.

However, the stress induced spectral shift is primarily dependent on the refractive index of the optical fiber N_f. Since both SCOS are coupled to the same optical fiber and are in close proximity, the spectra of both SCOS shift in the same direction with respect to both stress and temperature.

By subtracting the two signals from each SCOS the stress noise is significantly reduced while the electric field measurement amplitude is increased. Therefore, the resulting measured response eliminates a large portion of the noise.

To use this push-pull effect, the two lithium niobate crystals must be as close to each other as possible on the D-fiber and the signal for each SCOS needs to be separately measured. In this work the transmission spectrum of one of the SCOS is shifted such that the resonance of one SCOS lies in a relatively flat section of the other SCOS. The signals are then separated by using two lasers with different wavelengths. The wavelengths are chosen such that they lie respectively on one of the SCOS resonance edges. In this work the electric fields are small enabling the resonance edge to be assumed to be linear.

Equation (2-1) shows that the coupling wavelength depends on the thickness of the lithium niobate crystal, *t.* Therefore, the transmission spectrum of a SCOS can be shifted by changing the thickness of the crystal. The spectrum can also be shifted by adding a different material onto the crystal as long as the refractive index of the added material is larger than N_f. In order to shift the spectrum, silicon nitride is deposited onto a lithium niobate crystal prior to coupling it to the D-fiber.

2.3.1 Push-Pull SCOS Fabrication and Characterization

A layer of silicon nitride was deposited onto a lithium niobate crystal using Plasma Enhanced Chemical Vapor Deposition (PECVD) [31]. This altered crystal was then used to create a SCOS.

Figure 2-6 shows the normalized log scale transmission spectrum of the SCOS fabricated with the altered lithium niobate crystal overlaid with a representative transmission spectrum of a SCOS fabricated with an unaltered lithium niobate crystal. The resonances are shifted by approximately 3 nm.

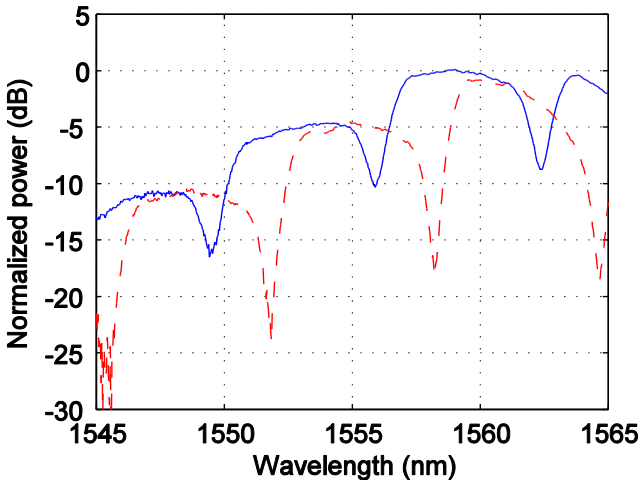

Figure 2-6: Normalized logarithmic SCOS transmission spectrum with (solid) lithium niobate crystal and (dashed) lithium niobate crystal with a layer of silicon nitride.

The push-pull SCOS was fabricated by coupling both the altered and unaltered lithium niobate crystals onto the same D-fiber. Figure 2-7 shows a picture of the push-pull SCOS. One of the crystals is notched to indicate which crystal has been altered with silicon nitride. If both crystals have their c axes in the same direction then the notched crystal is rotated 180 degrees.

Figure 2-8 shows the combined spectrum for the push-pull SCOS. The spectrum is essentially the multiplication of the two spectra shown in Figure 2-6. The first, third and fifth resonances with the lowest wavelength corresponds to the altered lithium niobate crystal and the other resonances are for the unaltered lithium niobate crystal.

To verify that both crystals have their optic axis flipped opposite to each other, the push-pull SCOS is mounted onto an interrogation stage. Figure 2-9 shows that the interrogation stage consists of a 10 mW tunable laser, electrodes spaced by 0.7 cm applying a 7.1 kV/m electric field across the push-pull SCOS, a photodiode, a TIA, and an oscilloscope.

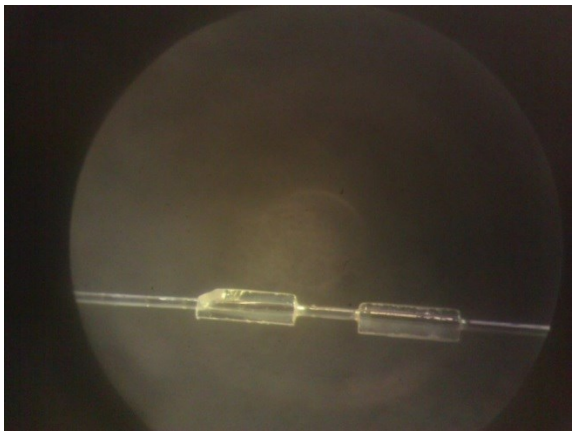

Figure 2-7: A push-pull SCOS with 2 lithium niobate crystals on a single D-fiber. One crystal is notched in the upper left corner to identify which crystal has been altered with silicon nitride.

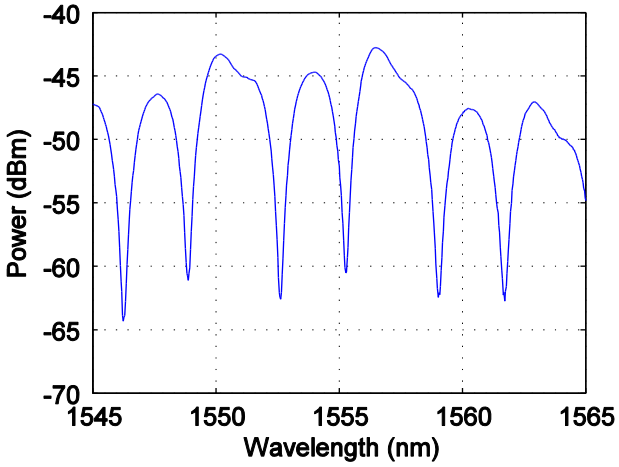

Figure 2-8: The push-pull SCOS has 2 lithium niobate crystals adhered to a single D-fiber, which causes a higher resonance dip frequency in the optical transmission spectrum.

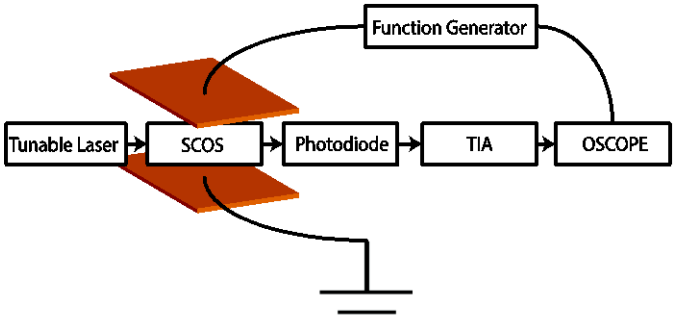

Figure 2-9: Push-pull SCOS interrogation setup.

A sinusoidal electric field is applied across the push-pull SCOS via the parallel plate electrode structure. The laser is tuned to have a wavelength of 1549 nm. Figure 2-8 shows that this wavelength lies on the rising edge of the resonance that corresponds to the SCOS fabricated with the uncoated lithium niobate crystal.

Figure 2-10(a) shows that the measured SCOS signal is in phase with the applied electric field signal. The laser is then tuned to a wavelength of 1546.6 nm and Figure 2-10(b) shows that SCOS signal is 180 degrees out of phase with the applied electric field signal. This confirms that the crystals have their optic axes flipped opposite to each other.

The calibration factor given in Equation (2-4) does not apply to Figure 2-10 since the SCOS is not yet connectorized at this point in the fabrication process. The important part about Figure 2-10 is to identify whether or not the optic axes are flipped opposite to each other.

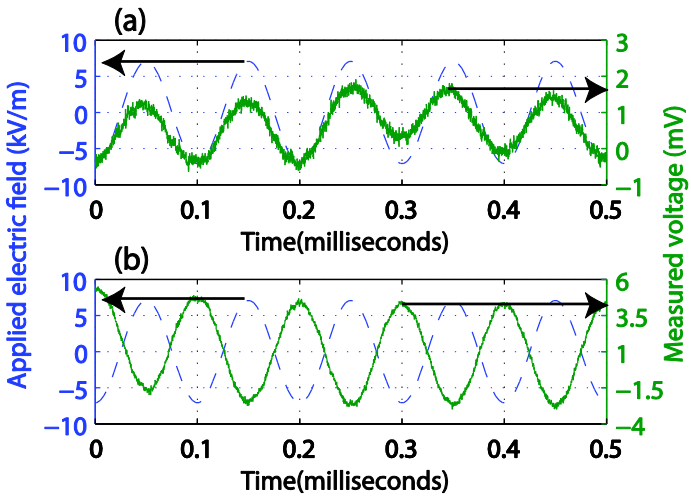

Figure 2-10: (a) Measured SCOS signal for uncoated crystal is in phase with applied electric field. (b) Measured SCOS signal is 180 degrees out of phase with applied electric field signal.

2.3.2 Electric Field Measurements

Figure 2-11 shows that the interrogation setup for the push-pull SCOS involves launching two lasers with wavelengths of 1549 nm and 1546.6 nm. These wavelengths correspond to the rising edge of the resonances of the two crystals. The two lasers are coupled into the push-pull SCOS using a polarization maintaining 50/50 fiber optic splitter/coupler. The SCOS is mounted on an impact stage that induces strain into the optical fiber of the push-pull SCOS.

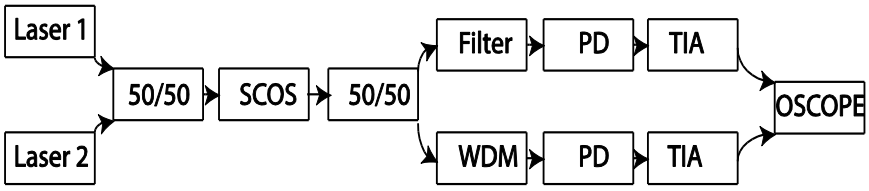

Figure 2-11: Push-pull SCOS interrogation setup.

To filter out the individual laser channels so that each photodiode reads an individual signal, the output of the push-pull SCOS is connected to another polarization maintaining 50/50 splitter. One output of the splitter leads to a LIGHTWAVE 2020 mechanically tunable optical filter, while the other leads to a WDM demultiplexer. A single channel of the WDM is used because the WDM pass bands do not match both channels. The LIGHTWAVE 2020 filter was used as the second pass band on the other side of the 50/50 splitter.

The outputs from the WDM and tunable filter each lead to an individual photodiode, where the optical signal is converted into an electrical current. The current is then converted into a voltage using a trans-impedance amplifier (TIA), and the voltage is captured by an oscilloscope.

Both lasers launched into the push-pull SCOS interrogation system have 10 mW of optical power. The components in the system reduce the final transmitted optical power dramatically. The optical signal power at the outputs of the WDM and tunable filter are on the order of tens of microwatts.

This loss is due to the fact that there is a total of 6 dB loss on each channel from the initial coupler and output splitter. The wavelength filters have losses of around 2 dB each. The SCOS itself has a loss of 2 dB per crystal and the laser is aimed at a resonance edge situated 3 dB below the maximum power level of the transmission spectrum. There are also losses between the couplings of the D fiber to the 50/50 couplers/splitters due to incompatible cores. All this power loss allows the TIA gain to be turned up to $A=10^6$ *V/A* 10^6in AC coupling mode without saturating any components. The TIA bandwidth is limited to 1 MHz via a selectable switch on the TIA. This is done to eliminate higher noise components such as thermal noise.

Figure 2-12 shows the impact stage setup to generate highly localized strain noise. The push-pull SCOS is attached to a bar that is hit by a swinging arm to ensure that the stage receives sufficient force to generate a recognizable amount of noise on the output signal.

The electrodes on both sides of the push-pull SCOS are attached to a signal generator to create a known electric field. The electrodes are suspended via an isolated arm that is not attached to the platform holding the impact stage. This prevents the field being applied across the push-pull SCOS from changing during impact measurements. The parallel plate electrode structure has a large enough area such that the field applied across the push-pull SCOS is homogeneous, in other words both crystals measure the same field.

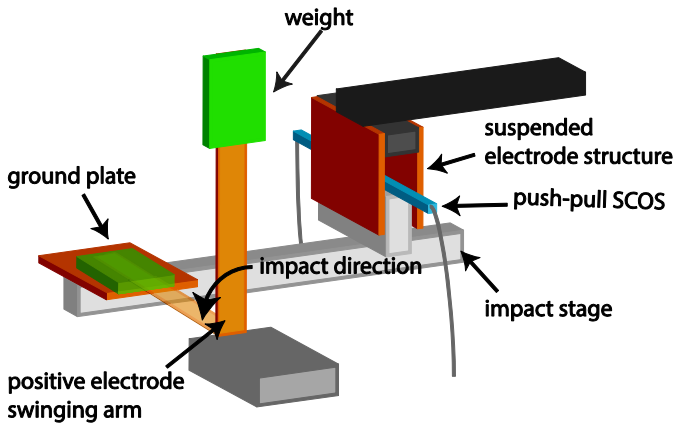

Figure 2-12: Impact stage setup for push-pull sensor. A positive electrode swinging arm impacts a ground plate attached to the impact stage which causes a short signal for the external trigger on the oscilloscope.

A series of pulses are applied to the electrodes. The pulses have amplitude of 200 volts and a repetition rate of 1 kHz. The electrodes have a separation of 2 cm resulting in a maximum applied electric field of 10 kV/m.

The repetition rate was chosen to be on the same order of frequency as initial strain measurements from the impact system. Pulses were chosen as the waveform because frequency filtering is not suitable to extract exponential pulses from noise which is on the same order of frequency since exponential pulses span a wide frequency range.

Figure 2-13 shows the output of the push-pull SCOS when the electric field is applied, without any strain. The two electric field signals are flipped opposite to each other corresponding to opposite wavelength shifts for the two lithium niobate crystals.

Figure 2-13 shows the two measured electric field signals that are attained by multiplying the measured voltage by the corresponding calibration factors given in Equations (2-3) and (2-4). It is important that both channels have the correct calibration factor during subtraction to attain the best strain noise reduction.

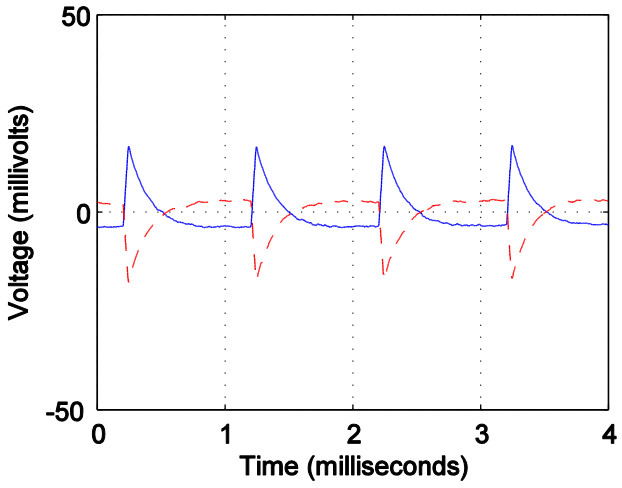

Figure 2-13: The push-pull SCOS consisting of two opposite electric field measurements, one from each lithium niobate crystal.

Figure 2-14 shows the result of subtracting the two electric field readings in Figure 2-13. As expected, the measured signal has doubled. The calibration for the push-pull SCOS with both channels taken into account is

$$E_m = 0.28 \frac{kV/m}{mV} V_m . \tag{2-5}$$

In this configuration, the lowest detectable field without vibration is 500 V/m while the lowest detectable field with vibration is 1000 V/m.

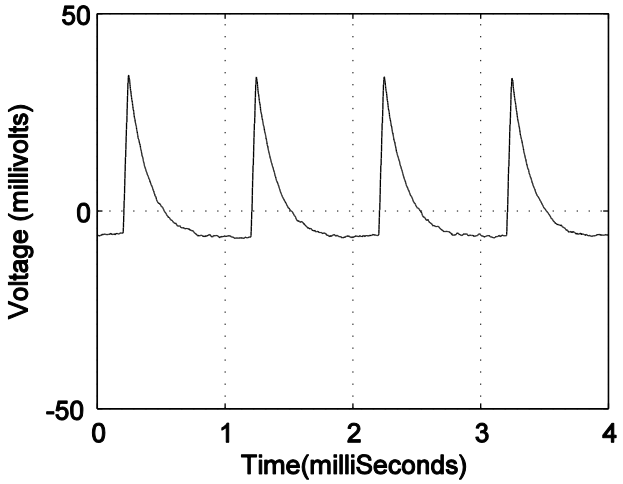

Figure 2-14: Subtracting the two opposite electtric field signals in Figure 2-13 preserves the electric field.

A slowly varying strain was applied to the push-pull SCOS by lifting the end of the impact stage up and down. The applied electric field from the previous figures are still present. Figure 2-15(a) shows the two measurements of the push-pull SCOS, and Figure 2-15 (b) shows the same signal zoomed in to a single period of the strain noise. Since the stress induced signal is larger than the electric field induced portion the two signals appear to be overlapped demonstrating that the signals track when the stress is the dominant signal.

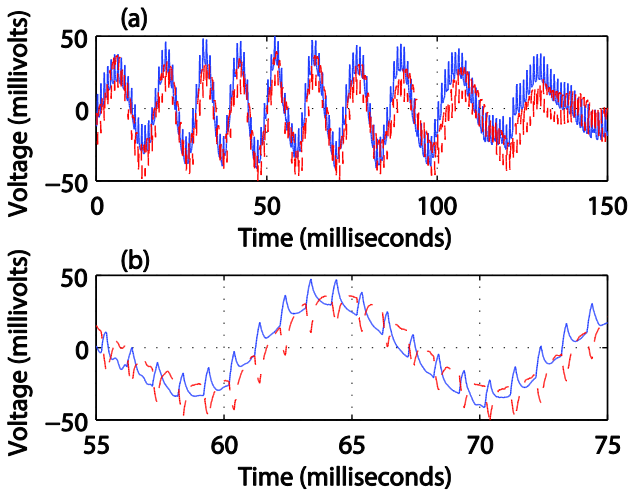

Figure 2-15: (a) Slow induced strain on the push-pull SCOS (b) Zoomed-in period of slow induced strain on push-pull SCOS.

As expected, Figure 2-16 shows that the majority of the stress induced signal is eliminated by subtracting the two signals. After subtracting, the electric field induced signal is larger than the stress induced portion.

Temperature induced stress on the fiber and crystal will have a similar effect to the slow strain measurements since temperature effects are inherently slow. As a result, a good portion of temperature induced stress noise can be subtracted by the same method as the slow strain noise.

The next test involved a higher speed impact event. The impact signal is a transient event. Therefore, the oscilloscope is triggered by the impact. The triggering is accomplished by placing a metal pad on the swing arm and the impact stage. When the swinging arm hits the impact stage arm a short is generated causing the oscilloscope to trigger.

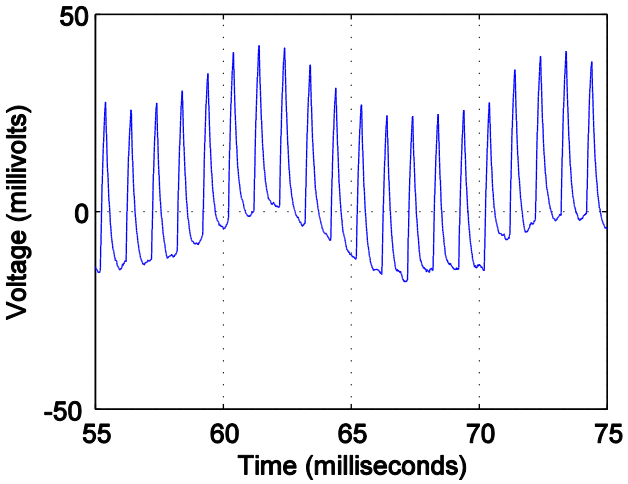

Figure 2-16: Subtracted stress signals reduced stress related signal and doubled electric field related signal.

Figure 2-17 shows measurements from the push-pull when the same electric field as in Figure 2-15 is applied across the push-pull SCOS with the stage impacted. The impact renders the exponential signals nearly unrecognizable.

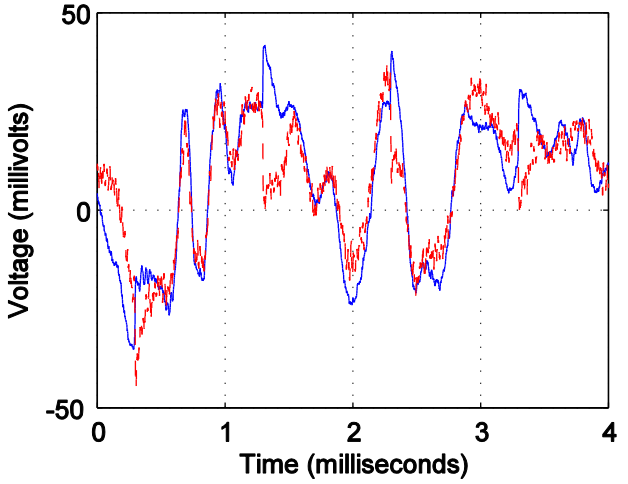

Figure 2-17: Vibration and electric field applied to the push-pull SCOS through two separate channels.

Frequency filtering could be applied to the low frequency strain signal; however, the impact causes the signal and the noise to span a similar frequency band. The push-pull SCOS provides a means to subtract the signals from the two sensors.

Figure 2-18 shows the subtracted signal. The periodic exponential signals can clearly be differentiated from the noise, allowing the shape and magnitude of the signal to be analyzed. No signal processing was used on Figure 2-18.

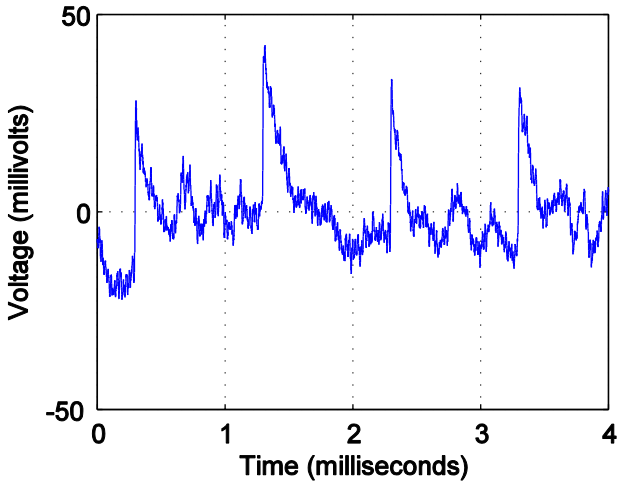

Figure 2-18: Subtraction of signals from Figure 2-17.

By performing additional signal processing such as a smoothing or filtering, it is possible to clean up the subtracted signal in Figure 2-18, allowing for a more usable, and potentially more accurate electric field reading to work with and to analyze.

2.4 Non-Localized Vibration Noise Reduction Method

In addition to the localized refractive index change described in the previous section, vibrations also change the refractive index along random lengths of optical fiber resulting in the phase change of the optical signal. Typically, this phase change does not add noise to the system

since the optical detector is only intensity based. However, Figure 2-19 shows that at fiber optic connection points, multiple reflections lead to multiple time shifted replicas of the same optical carrier propagating down the same fiber. These multiple reflections paired with the random phase fluctuations due to vibration on random segments of the optical fiber lead to excessive interferometric noise [35][36].

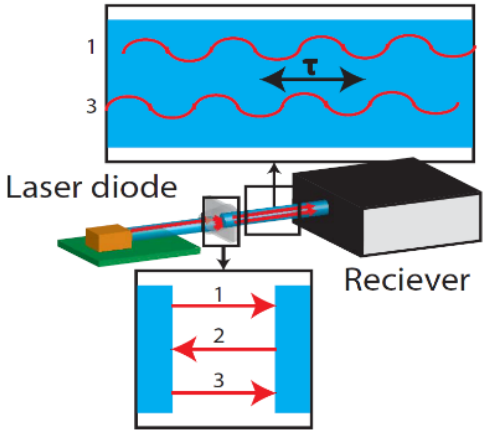

Figure 2-19: Multiple reflections at fiber connection points cause time shifted replicas of the optical carrier to propagate down the same fiber.

2.4.1 Interferometric Noise Background

The basic analysis of interferometric noise has already been derived [37]; however, a summary of this derivation is provided for convenience. This summary only considers a dominant time shifted signal which is not necessarily true in all cases, but proves to be simple and highly effective in this work, and continues to be effective when applied to recent SCOS measurements and applications. The derivation begins by considering the multiple reflections

that causes the detected signal to be the original signal combined with a time shifted version as given by

$$E_{out} = E(t) + \psi\, E(t-\tau) \quad , \tag{2-6}$$

where *E(t)* is the electric field of the original signal, ψ is the magnitude of the double reflection, and τ is the time shift caused by the double reflection at a fiber optic connection point.

The multiple reflection causes the detected signal intensity at the photodetector to become

$$I_{\det} = E_{out}E_{out}^{*} = \left|E(t)\right|^2 + 2\psi\,\mathrm{Re}\left\{E(t)E^{*}(t-\tau)\right\} + \psi^2\left|E(t-\tau)\right|^2 . \tag{2-7}$$

The first term in Equation (2-7) is the signal, the second term is the noise, and the third term is neglected because $|\psi| \ll 1$.

The electric field of the signal is given by

$$E(t) = \sqrt{P_o\, d(t)}\exp\left(j\left[\omega_{op}t + \phi(t)\right]\right) \tag{2- 8}$$

where P_o is the average laser power, *d(t)* is the change in the laser power caused by the sensing element, ω_{op} is the optical carrier frequency, and $\phi(t)$ is the phase noise. Inserting Equation (2-8) into Equation (2-7) results in signal intensity of

$$I_s \approx P_o\, d(t), \tag{2-9}$$

and noise intensity of

$$I_n = 2\psi\, P_o\sqrt{d(t)d(t-\tau)}\cos\left(\omega_{op}\tau + \phi(t) - \phi(t-\tau)\right), \tag{2-10}$$

where

$$\Delta\phi(t) = \phi(t) - \phi(t-\tau) \tag{2-11}$$

is the phase noise term.

The power spectral density of the noise depends on the specific time variation of both the signal *d(t)* and the phase noise $\phi(t)$. However, we can generalize both of these signals to be band limited signals. The resulting generalized power spectral density of the noise is given by [37]

$$S_N(f) = 2\psi^2 P_o S_{sig} \otimes S_\phi, \tag{2-12}$$

where S_{sig} is the power spectral density of the signal and s_ϕ is the power spectral density of the phase noise, and $\otimes$ denotes convolution. The vibration induced interferometric noise is reduced by up conversion to a higher frequency band that enables the noise to be filtered out without removing the desired signal [38].

The phase modulation changes the electric field of the signal to

$$E(t) = \sqrt{P_o\, d(t)} \exp\left(j\left[\omega_m t + \phi(t) + k\cos(\omega_m t)\right]\right), \tag{2-13}$$

where ω_m is the phase modulation frequency and *k* is the index of modulation given by [39][40]

$$k = \pi \frac{V_{app}}{V_\pi}, \tag{2-14}$$

where V_{app} is the applied peak voltage from the RF generator, and V_π is the half wave voltage amplitude of the phase modulator quoted to be 3.5 V [41]. Therefore, the estimated *k* used in this work is

$$k = \pi \frac{2.5}{3.5} = 2.244. \tag{2-15}$$

The noise intensity is found using the same process as before resulting in

$$I_n = 2\psi P_o \sqrt{d(t)\,d(t-\tau)}\,\mathrm{Re}\left\{\exp\left(j\omega_{op}\tau + j\Delta\phi + jK\right)\right\}, \tag{2-16}$$

where

$$K(t) = -2k\sin\left(\frac{\omega_m \tau}{2}\right)\sin\left(\omega_m t - \frac{\omega_m \tau}{2}\right). \tag{2-17}$$

The term e^{jK} can be simplified using the Jacobi-Anger identity

$$e^{j\alpha\sin\theta} = \sum_{q=-\infty}^{\infty} J_q(\alpha) e^{jq\theta}, \tag{2-18}$$

to become

$$e^{jK} = \sum_{q=-\infty}^{\infty} J_q\left(-2k\sin\left(\frac{\omega_m \tau}{2}\right)\right)\exp\left(jq\left[\omega_m t - \frac{\omega_m \tau}{2}\right]\right). \tag{2-19}$$

Inserting Equation (2-19) into Equation (2-16) results in a noise intensity of

$$\begin{aligned} I_n &= 2\psi P_o \sqrt{d(t)\,d(t-\tau)} * \sum_{q=-\infty}^{\infty} J_q\left(-2k\sin\left(\frac{\omega_m \tau}{2}\right)\right) \\ &* \mathrm{Re}\left\{\exp\left(j\omega_{op}\tau + j\Delta\phi + jq\,\omega_m t - jq\,\frac{\omega_m \tau}{2}\right)\right\} \end{aligned} \tag{2-20}$$

,

which can be simplified to

$$\begin{aligned} I_n &= 2\psi P_o \sqrt{d(t)d(t-\tau)} * \sum_{q=-\infty}^{\infty} J_q\left(-2k\sin\left(\frac{\omega_m \tau}{2}\right)\right) \\ &* \cos\left(\omega_{op}\tau + \Delta\phi(t) + q\,\omega_m t - q\,\frac{\omega_m \tau}{2}\right) \end{aligned} \tag{2-21}$$

.

The cosine term in Equation (2-21) is similar to a phase modulated communications signal [42]. In a phase modulated communication signal the frequency spectrum is centered on the phase modulation term $q\omega_m$.

Thus, the phase modulator converts the vibration induced interferometric noise into a set of frequency bands centered at frequencies of $q\omega_m$. Figure 2-20 shows the first three frequency bands. Low-pass filtering the signal eliminates all of the vibration induced interferometric noise terms except for the $q=0$ term. The photodetector and TIA are the primary low pass filters in the system since the TIA only has a bandwidth of a few MHz.

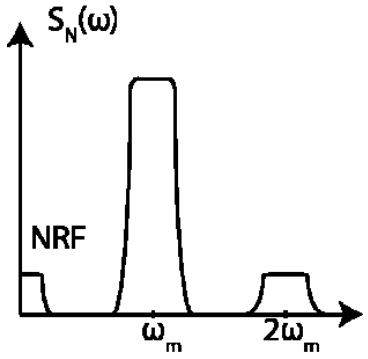

Figure 2-20: Distribution of the noise power among different harmonics after phase modulation.

The remaining $q=0$ term is the reduction in the vibration induced interferometric noise and is called the noise reduction factor (NRF) and is given by

$$NRF = J_o^2\left(-2k\sin\left(\frac{\omega_m \tau}{2}\right)\right) \quad . \tag{2-22}$$

The time delay τ is determined by the sensor system setup. Thus, there are two control parameters in Equation (2-22) namely the frequency of the modulator ω_m, and the modulation index *k*.

Figure 2-21 shows the NRF simulated as a function of both the modulation index *k* and the modulation frequency times the time delay $\omega_m\tau$. This figure shows that there are a repeating set of regions where the NRF is equal to 1 meaning that there is no reduction in the noise. These regions occur at

$$\omega_m \tau = 2\pi n, \tag{2-23}$$

where *n* is any integer. The greater the modulation index *k* the wider the range of frequencies with good NRF, therefore the maximum possible value of *k* was used in this work which estimates an NRF of approximately 0.11 when taken from *1/2n* to *n*.

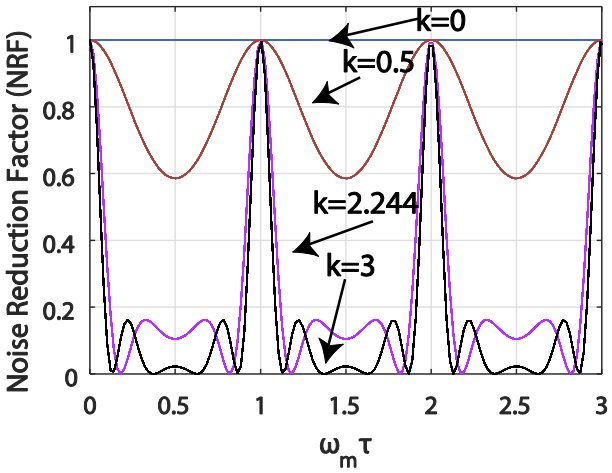

Figure 2-21: Noise reduction factor (NRF) as a function of the normalized modulation frequency, $\omega_m\tau$. There are certain modulation frequencies at which there is no noise reduction.

Multiple time domain shifted signals will require a range of ω_m to up convert noise from multiple reflections. To do this, a wide band phase modulation with a bandwidth of a few hundred megahertz is used rather than a single tone phase modulation. However, this requires a broadband RF source which is not obtainable by the authors of this work. Single tone phase modulation has proven to be very effective and simply for this application.

Only PM fiber is used in these experiments due to the polarization dependent nature of the SCOS. Therefore, the NRF is not affected by changing polarization states of the output spectrums of the laser.

So far, the analysis of localized vibrational noise reduction, RF noise reduction and non-localized vibrational noise reduction has been analyzed. The next section introduces the harsh environment used in this work as well as the results from the applications of the noise reduction techniques.

2.4.2 Implementation of Non-Local Vibration Induced Noise Reduction in SCOS

Figure 2-22 shows that this approach requires single tone phase modulating the optical carrier by using an external phase modulator driven by an RF generator. The phase modulator used in these experiments is a custom LN53S-FC from Thorlabs (Newton, NJ) with polarization maintaining fiber (PM) on the input and output for interrogation of the r_{33} coefficient of the lithium niobate crystal. The phase modulator is driven with an N9310A RF generator from Agilent. The measured amplitude was approximately 5 V peak to peak with a frequency that was varied between 2 GHz and 3 GHz.

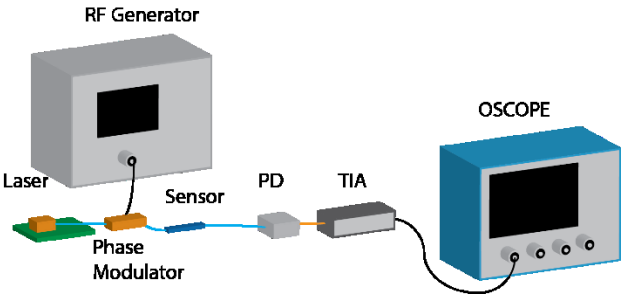

Figure 2-22: By phase modulating the optical carrier before feeding into the SCOS, interferometric noise due to random vibrations along the length of the fiber can be up-converted.

Figure 2-23 (a) shows that with no vibration, interferometric noise can still overwhelm the electric field measurements for low electric fields. The electric field is applied in this measurement but cannot be differentiated from the noise. Figure 2-23(b) shows the Fourier transform for Figure 2-23(a), which indicates a majority of the interferometric noise is centered around 22 kHz. This periodic noise is caused by the phase fluctuation of the tunable laser that is converted into intensity noise by the multiple reflection interference [43].

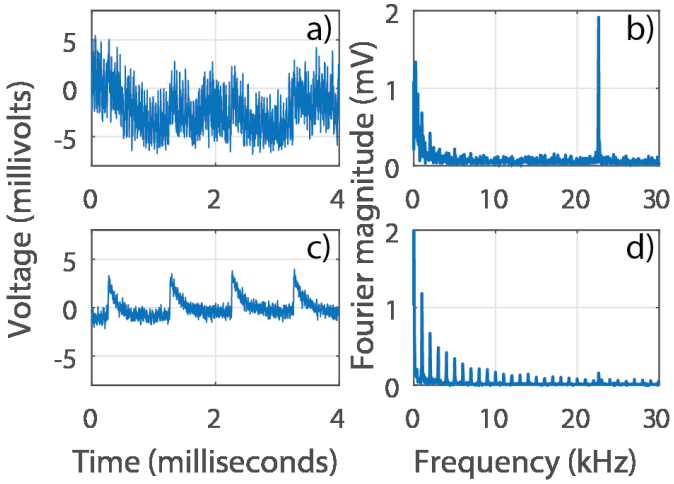

Figure 2-23: (a) Measurement of the low vibration system without phase modulation. (b) Fourier transform of the low vibration system without phase modulation. (c) Measurement of the low vibration system when phase modulation is applied. (d) Fourier transform of the low vibration system with phase modulation.

Figure 2-23 (c) shows that by up-converting the interferometric noise through phase modulation, that the desired electric field signal can be obtained. Figure 2-23 (d) shows the Fourier transform of Figure 2-23 (c), the periodic spikes correspond to the Fourier transform of periodic exponentials.

By monitoring the amplitude of the interferometric noise spike at 22 kHz in Figure 2-34(b) as ω_m is varied, it is possible to locate the best NRF for a given ω_m. Figure 2-24 shows a sweep of the NRF as a function of ω_m using a laser through a push-pull channel. The spectrum does not match Figure 2-21 precisely likely due to multiple double reflections, but the NRF valleys can be identified for a single dominant time shifted signal, therefore a suitable single tone modulation location can still be found. For this particular push-pull channel an f_m of 2.906 GHz was used to achieve an NRF of 0.11, which agrees well with the simulation in Figure 2-21.

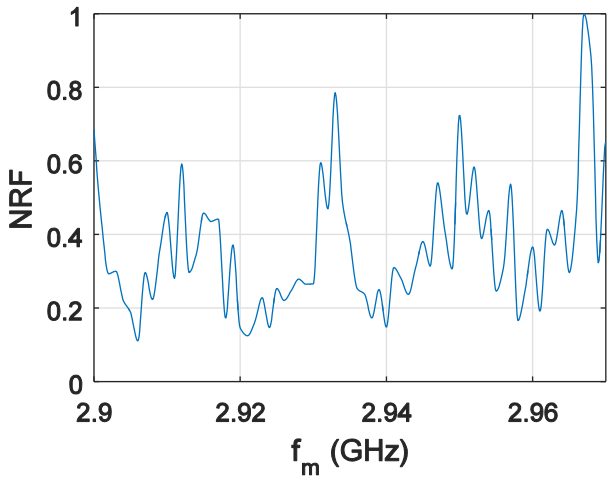

Figure 2-24: A suitable NRF can be found by sweeping f_m and choosing the best NRF.

Vibration is applied by simply moving a random section of the optical fiber. Figure 2-25(a) shows the interferometric noise induced from moving the optical fibers. Figure 2-25(b)

shows the Fourier transform of Figure 2-25(a) and shows that the interferometric noise has a frequency content that is much higher than the actual movement rate of the optical fiber.

Using the same ω_m applied in Figure 2-23. Figure 2-25(c) shows that the electric field signal can be recovered by up-converting the interferometric noise caused by the fiber motion. Figure 2-25(d) shows the Fourier transform for Figure 2-25(c), and indicates that a majority of the interferometric noise induced by the harsh environment has been up converted and filtered out.

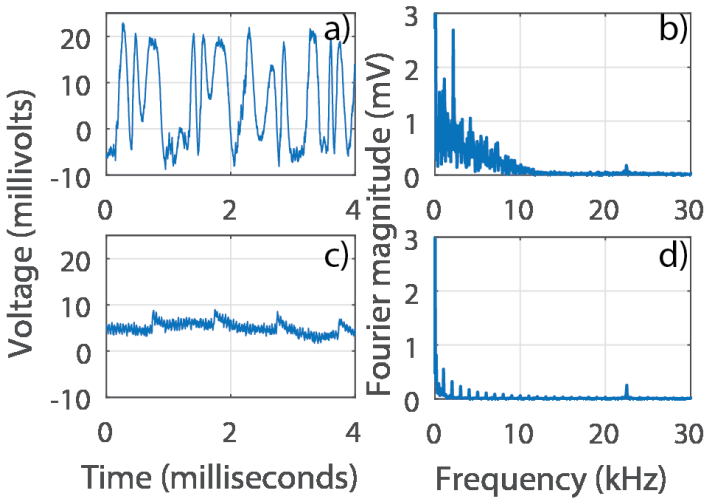

Figure 2-25: (a) Measurement of the slow vibration system without phase modulation. (b) Fourier transform of the slow vibration system without phase modulation. (c) Measurement of the slow vibration system when phase modulation is applied. (d) Fourier transform of the slow vibration system with phase modulation.

2.4.3 Non-Localized Noise Reduction in Fiber Bragg Grating Sensor

To illustrate the effects of interferometric noise in other fiber optic sensors, this section shows interferometric noise reduction on a fiber Bragg grating (FBG). Figure 2-26 shows that a FBG is

a section of optical fiber with a periodic variation in the refractive index of the core. The FBG reflects a specific wavelength as given by

$$\lambda_B = 2n_e\Lambda, \tag{2-24}$$

where λ_B is the reflected wavelength called the Bragg wavelength, n_e is the effective refractive index of the optical fiber mode and Λ is the grating period.

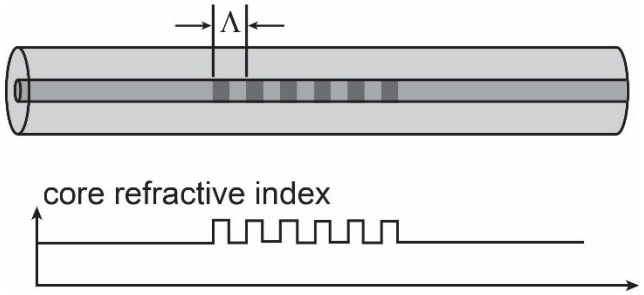

Figure 2-26. Cross sectional figure of a fiber Bragg grating.

When the FBG is strained it causes a change in both the grating period Λ and the effective index of refraction of the fiber mode n_e resulting in a shift of the transmission spectrum. For an FBG written in a standard optical fiber the shift is $1.2\ pm/\mu\varepsilon$ [44] .

Very small strain can be measured by tuning a laser to have a wavelength that lies on the edge of the transmission dip. Small shifts in the spectrum result in changes in the transmitted optical power. This type of FBG interrogation is called FBG edge detection[45][46] .

Figure 2-27 shows the measured FBG spectrum obtained by tuning the laser across the wavelength band from 1549 nm to 1551 nm. With a laser tuned to a wavelength of λ=1550.12 nm the slope of the resonance is

$$\frac{\Delta V}{\Delta\lambda} = 115.55\frac{mV}{pm}. \tag{2- 25}$$

Using the FBG shift of *1.2 pm/με*, the resulting sensitivity is

$$\frac{\Delta V}{\Delta \varepsilon} = 138.66 \frac{mV}{\mu\varepsilon}. \tag{2-26}$$

Figure 2-28 shows that the FBG measurement setup consists of an FBG attached to a foam board using Devcon 5 minute epoxy. The board is attached to solid platforms at both ends to prevent excessive movement. A piezoelectric transducer (PZT) is attached using 3M industrial double sided tape to the foam board. The PZT is driven with a sinusoidal signal with a frequency of 2 kHz.

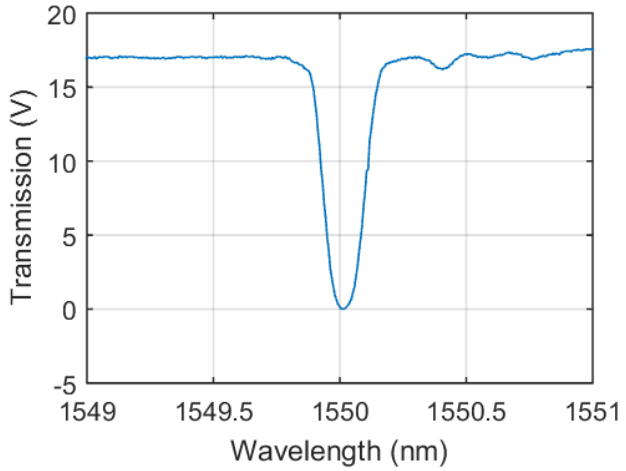

Figure 2-27. The measured FBG spectrum.

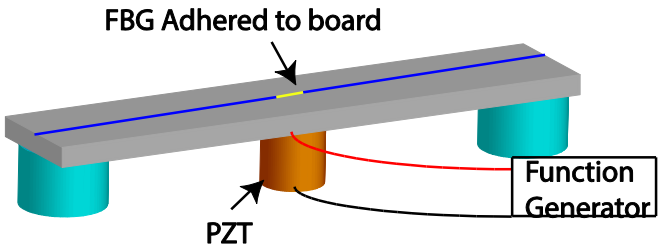

Figure 2-28. The FBG measurement system.

Figure 2-29(top) shows the FBG measurements before external phase modulation of the optical source. Since the FBG measurement uses different lengths of optical fiber than the SCOS

measurement it has a different value for τ. The different value for τ required that the phase modulation frequency be adjusted to approximately 3 GHz to attain a sufficient NRF. Figure 2-29 shows that with the phase modulation the noise is reduced by a factor of 25.

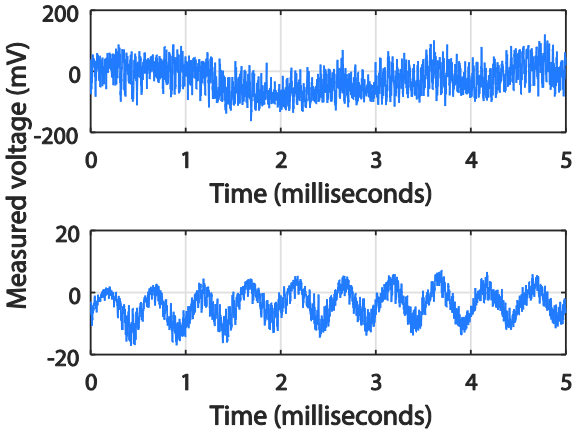

Figure 2-29. FBG measurement (top) before phase modulation, and (bottom) after phase modulation.

Figure 2-30 shows the Fourier transform of the FBG measurement. Similar to the SCOS measurement, there is an interferometric noise spike at 22 kHz caused by the laser phase noise. With the phase modulator the interferometric noise has been reduced enough to enable the 2 kHz strain signal to be measured. With the reduction in the interferometric noise the 2 kHz strain signal is measured to have an amplitude of 14 mV, which corresponds to a strain with an amplitude of 0.1 με.

Figure 2-31 shows the FBG measurement when a manual vibration is applied to the FBG output fiber. The noise is reduced by a factor of 26. Figure 2-32 shows that the noise has been reduced dramatically and the Fourier spectrum essentially only contains the 2 kHz sinusoid signal.

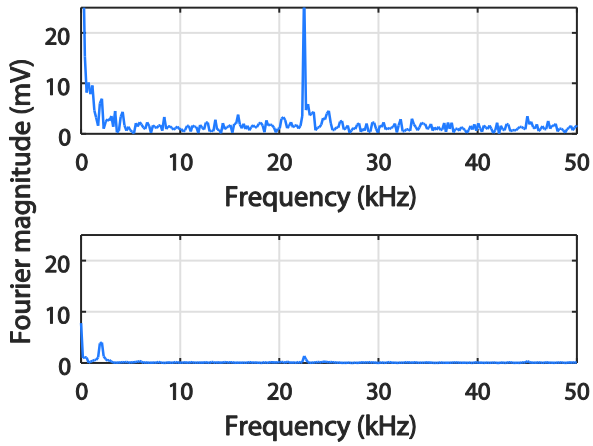

Figure 2-30. Fourier transform of FBG measurements in Figure 2-29 (top) before phase modulation, and (bottom) after phase modulation.

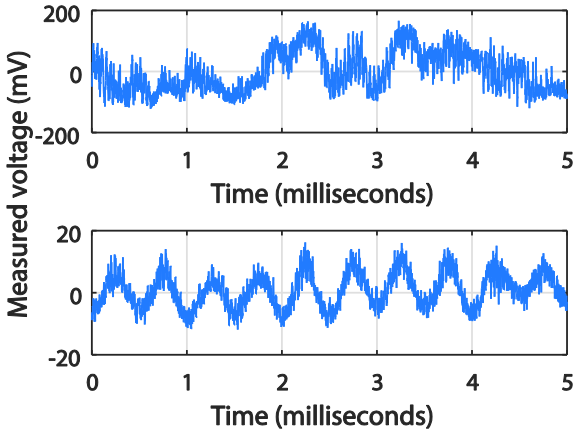

Figure 2-31. (top) measurement with FBG in a dynamic environment without phase modulation and (bottom) with phase modulation.

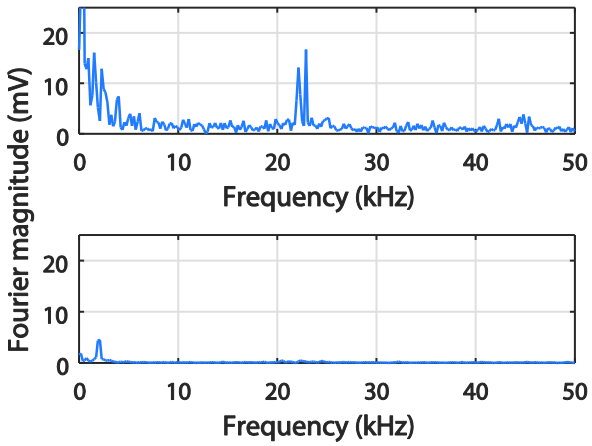

Figure 2-32. Fourier transform of FBG measurements in Figure 2-31 (top) before phase modulation, and (bottom) after phase modulation.

2.5 Experiment and Results

2.5.1 Harsh Environment Setup

The harsh environment used in this work induces three separate noise types onto the SCOS simultaneously, non-localized vibration noise, localized vibration noise, and RF noise. This section shows how to eliminate all three noise types to achieve an electric field measurement in a harsh environment.

The push-pull SCOS is packaged in a casing with parallel plate electrodes attached on both sides to generate an electric field. A positive and negative terminal is then connected to the electrodes from a voltage source.

Figure 2-33 shows the apparatus used to simulate a harsh environment that would cause vibration noise to the sensor itself as well as along random sections of optical fiber and RF noise. It is a large swinging arm that measures 1.5 meters in length.

The swinging arm has a loose hinge system at its origin to guarantee that it can create vibrational noise in all directions rather than just in the vertical direction. The swinging arm triggers the oscilloscope on impact by connecting two contacts on its free end. The push-pull SCOS is directly mounted on the swinging arm with an electric field applied in the direction of the optic axes of the crystals, perpendicular to the swinging direction of the arm. Medical tubing is attached between the surface that the arm is mounted on and the free end of the swinging arm. This causes the swinging arm to impact the contacts with much more force than occurs with free fall. This also creates a significant amount of acoustic noise during impact.

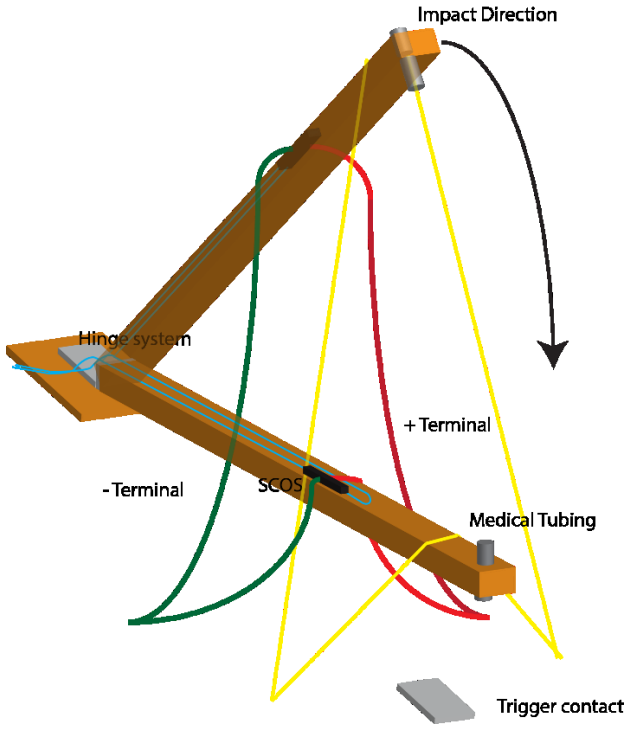

Figure 2-33: Swinging arm apparatus used to apply random vibration noise to the sensor and sections of fiber attached to the sensor. The data acquisition system is triggered via a trigger contact on the large swinging arm.

A voltage is applied to the electrodes placed on the sides of the SCOS to generate an electric field. Figure 2-34 shows the voltage applied to the electrodes, which are spaced by *18.5 mm*. The resulting applied electric field is a periodic set of exponential pulses with amplitude of *10 kV/m*.

This harsh environment has a much larger vibration than simply moving the optical fiber. The large vibration is created by impacting the bar into the trigger contact. This impact creates a range of vibration frequencies as well as amplitudes. The impact causes vibration in a large length of optical fiber as well as localized to the SCOS itself. It also creates acoustic noise that can cause stress in both the SCOS and the optical fiber.

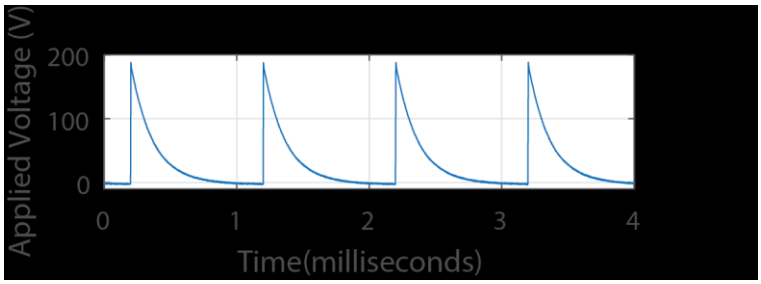

Figure 2-34: The voltage signal applied to the electrodes placed on the sides of the SCOS

2.5.2 Harsh Environment Noise Reduction

Ensuring than an appropriate ω_m is chosen for both channels of the push-pull SCOS, localized vibration noise as well as RF noise is subtracted. Figure 2-35(b) shows the measured electric field signal on both channels without phase modulation. The vibration induced interferometric noise on both channels is uncorrelated, therefore a subtraction would not lead to the desired electric field measurement.

Figure 2-35(c) shows the measurement on both channels with phase modulation. The interferometric noise induced by the harsh environment is now up-converted and both channels of the push-pull configuration are able to track the strain noise local to the sensing element. Since the optic axes of the crystals are flipped in opposite directions, the electric field tracks in opposite directions but strain noise tracks in the same direction. Figure 2-35(d) shows that the electric field signal can be recovered by subtracting the two channels from the push-pull. It is uncertain whether the residual noise is due to vibrations induced on the electrodes applying the electric field or is actual residual vibrational noise.

Many of the systems that need to have their electric field characterized also produce a noticeable amount of radio frequency (RF) noise which needs to be reduced. RF noise can be generated through voltage contact triggers or through any operation of the system that creates an electric discharge [47][48][49]. While the optical fiber sensor itself is immune to RF noise, the measurement electronics interrogating the sensor are not.

RF noise is noticeable at shorter time periods as a damped oscillation. Figure 2-36(a) shows the applied 10 kHz periodic exponential signal measured from the harsh environment and Figure 2-36(b) shows the measured signal on both channels of the push-pull configuration. The localized strain noise is not noticeable at this time period because it is too slow; however, if it were fast enough, the push-pull would be able to reduce it.

The vibration induced interferometric noise has been up-converted but the rise time of the periodic exponential cannot be analyzed due to RF noise. With the RF noise, it is uncertain whether the initial rise is due to RF noise or is part of the electric field signal. Figure 2-36(c) shows that by subtracting the two channels of the push-pull, the RF noise can be reduced and more features of the electric field signal can be analyzed.

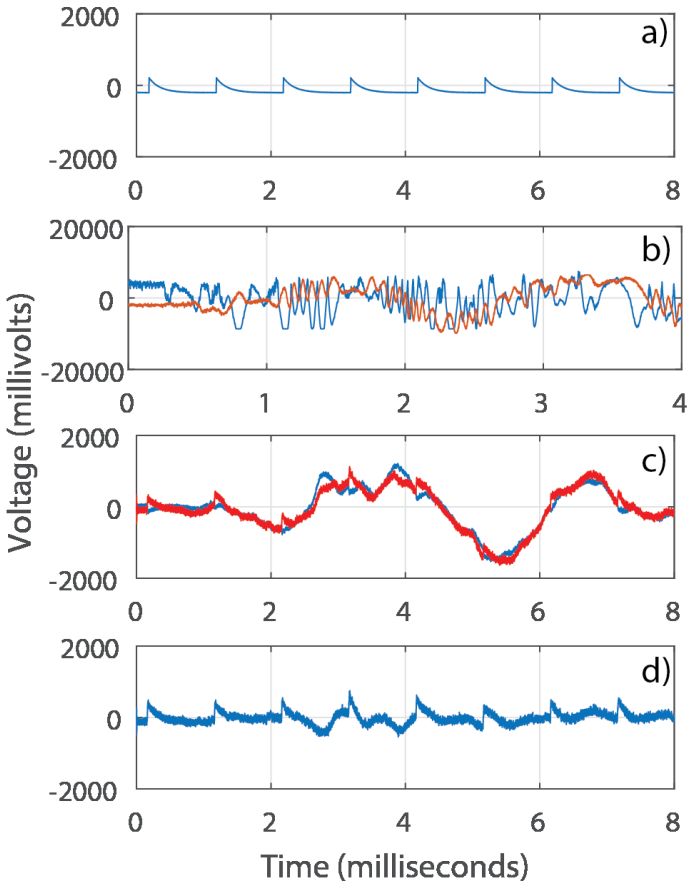

Figure 2-35: (a) Electric field applied to the push-pull SCOS. (b) Measured electric field from harsh environment on two channels without phase modulation (c) Measured electric field on two channels with phase modulation. (d) Subtraction of the two signals.

Figure 2-37 shows a zoomed in image of Figure 2-36(b) to show the tracking on both channels of the push-pull SCOS. Both channels are able to track the RF noise well enough to allow for an effective subtraction that takes out a good portion of the RF noise.

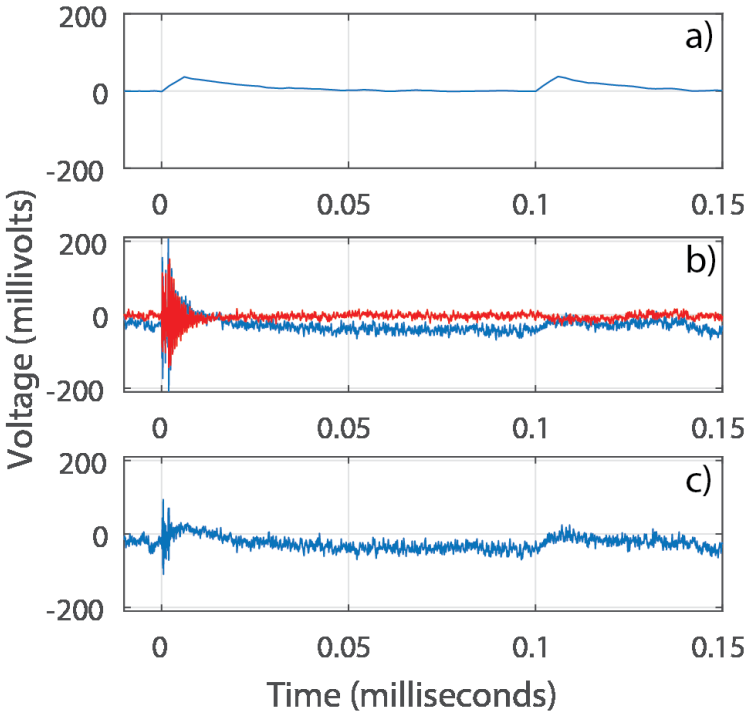

Figure 2-36: (a) Electric field applied to the SCOS. (b) Measured signal from the two SCOS sensing elements. (c) Subtraction of the two SCOS signals.

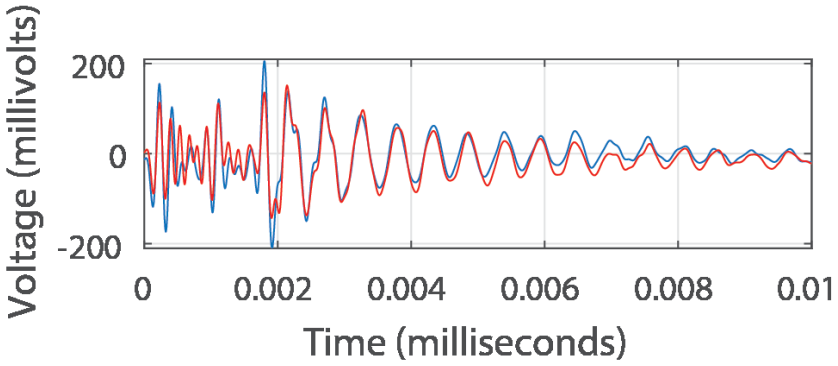

Figure 2-37: Zoomed-in image of Figure 2-36(b), the RF noise on both channels track, allows for a push-pull subtraction of the RF noise.

2.6 Summary

Fiber optic sensors in harsh environments must be able to overcome all the noise types simultaneously in order to obtain a proper measurement. This work has illustrated that by independently single tone phase modulating each optical carrier channel of the push-pull SCOS, it is possible to eliminate non-local vibration noise which manifests itself as interferometric noise. This allows for effective use of the push-pull SCOS configuration, which drastically reduces local vibration noise to the sensing element and RF noise, which manifests itself as damped oscillations for shorter time periods.

The setup used in this work is capable of eliminating all three noise sources individually or simultaneously. This allows for the SCOS to measure electric fields in a harsh environment.

3 SPLIT HOPKINSON BAR MEASUREMENT USING HIGH-SPEED FULL-SPECTRUM FIBER BRAGG GRATING INTERROGATION

3.1 Optical Measurement Setup

Figure 3-1 shows that an FBG is a section of optical fiber with a sinusoidal periodic variation in the refractive index of the core. The FBG reflects a specific wavelength as given by

$$\lambda_B = 2n_e\Lambda \quad , \tag{3-1}$$

where λ_B is the reflected wavelength called the Bragg wavelength, n_e is the effective refractive index of the optical fiber fundamental mode and Λ is the grating period.

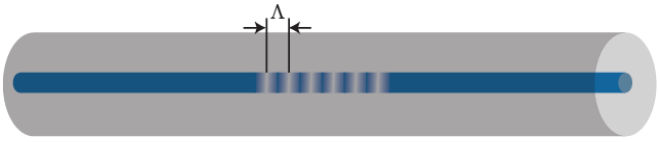

Figure 3-1: Fiber Bragg grating that consists of a periodic change Λ in the refractive index of the core. This periodic change reflects a specific wavelength called the Bragg wavelength λ_B.

Figure 3-2 shows a sample spectrum of the ratio of powers (R), where the peak of the reflected spectrum corresponds to the Bragg wavelength given by Equation (3-1). A strain applied to the FBG causes a change in both the grating period, Λ, and the effective index of refraction of the fiber mode, n_e, resulting in a shift of the λ_B. A Micron Optics os1100 FBG is used in this work has a strain sensitivity of 1.2 pm/με [50] .

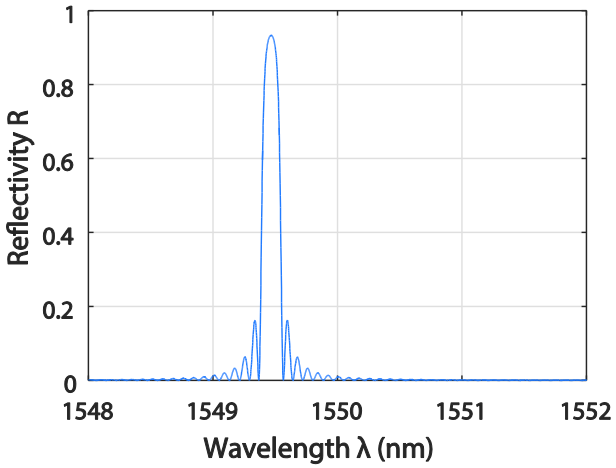

Figure 3-2: Reflection spectrum for an FBG. The peak of the reflected spectrum λ_B will change due to thermal and strain effects on the FBG.

3.2 High-Speed Full-Spectrum Interrogation

For this test, an Insight Photonics Solutions model SLE-101 swept laser source was used to interrogate the FBG [51]. This solid state swept laser source can sweep 100 kHz with a 40 nm sweep band centered on 1544 nm. In this work, a sweep band from 1534 nm to 1564 nm is used with a repetition rate of 100 kHz.

Figure 3-3 shows that the laser works by alternating the semiconductor laser's refractive index by regulating the current flow through it. By controlling and synchronizing the currents flowing, the laser can be controlled very precisely. Elements a and d are distributed Bragg reflectors, b is the cavity gain medium unit, c is the cavity length adjustment unit, and e is a semiconductor optical amplifier unit. The current changes the refractive indices of the two mirrors, which allows for a different feedback wavelength to be selected. This tuning is made finer by adjusting the cavity length.

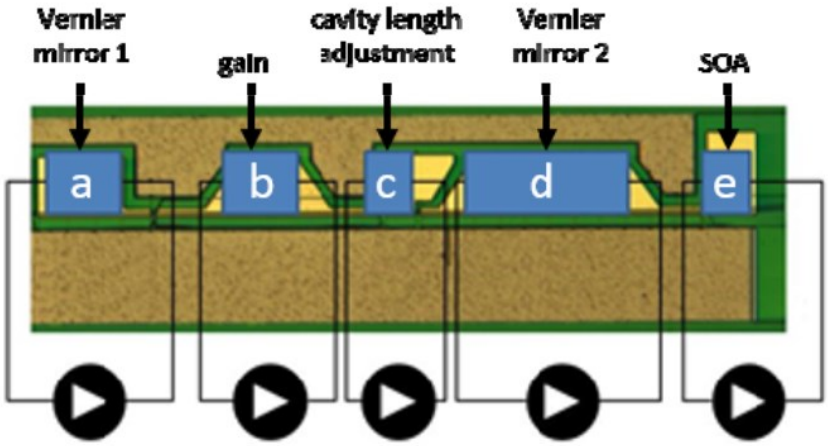

Figure 3-3. Schematic representation of Insight laser cavity [51].

Figure 3-4 shows that the swept laser source feeds into a fiber optic circulator. The reflected spectrum from the FBG is captured by a photodiode (PD) as a time domain signal, where the time is directly related to the sweeping wavelengths of the source. The photodiode converts the optical power from the FBG spectrum into an electrical current. The electrical current is then converted into a voltage using a variable gain transimpedance amplifier (TIA). The time domain waveform is then captured by an oscilloscope (OSCOPE).

Figure 3-5 shows the process diagram for converting the captured time domain FBG waveform from the oscilloscope into a wavelength domain waveform. A linear sweep in wavelength is initiated on every rising and falling edge of the captured clock signal while simultaneously terminating the previous sweep. By knowing the starting sweep wavelength and the ending sweep wavelength, the spectrum in terms of wavelength can be recovered from the time domain spectrum by relating the start sweep/end sweep signal to the captured spectrum, and linearly mapping the captured data points to the linearly swept wavelengths. By plotting a false

color representation of the captured FBG spectra over time, it is possible to observe the spectrum shifts and deformations over time.

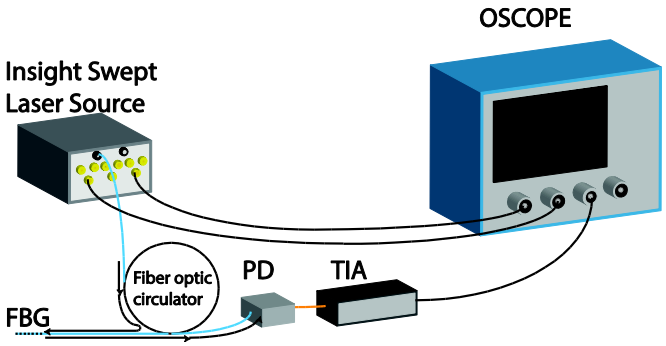

Figure 3-4: Optical setup for full-spectrum high-speed interrogation of an FBG. A swept laser source feeds into the input port of a fiber optic circulator. The transmission port of the circulator feeds to the FBG being interrogated. The reflected spectrum is routed through a circulator to a photodiode (PD) and then to a transimpedance amplifier (TIA), and the voltage signal is captured by the oscilloscope (Oscope).

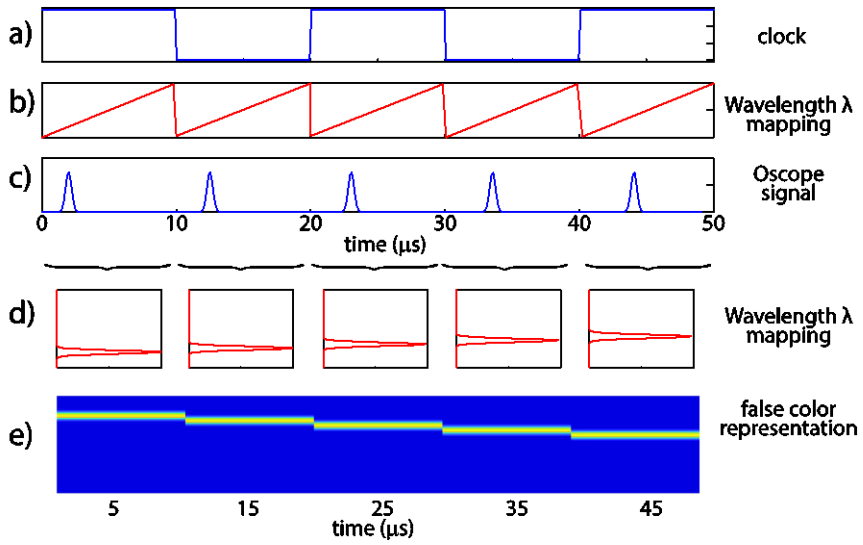

Figure 3-5: (a) A rising/falling clock edge initiates (b) a new sweep linear in wavelength. (c) The time domain waveform is converted into (d) a time varying wavelength spectrum, which can be represented by (e) a false color representation.

Figure 3-6 (solid red line) shows the measured waveform from the FBG as well as (dashed blue line) the start sweep and end sweep signal from the laser. This shows that by using

high-speed full-spectrum interrogation, it is possible to observe the nonlinear strain deformation of the FBG spectrum over time. Using this information, it is possible to reconstruct the strain distribution profile on the FBG through optimization using the transfer matrix approach [16][17].

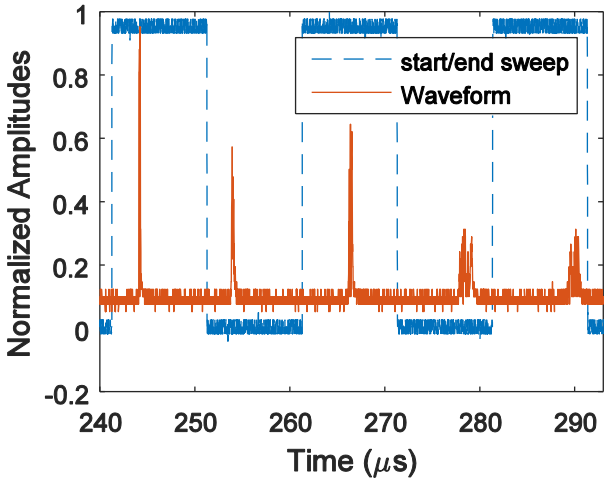

Figure 3-6: (dashed blue line) A new sweep initiates every rising/falling clock cycle capturing (solid red line) nonlinear strain deformations in the FBG spectrum over time.

3.3 Strain Calculations

To obtain strain profile information along the FBG from the measured reflection spectrum, an optimization procedure was applied that involves generating simulated deformed reflection spectra given strain profiles. These predicted reflection spectra are then compared against the actual measured spectrum.

Many different optimization algorithms have been developed to obtain the distributed strain profile through an FBG [16][17]. An efficient approach for calculating the reflected spectrum of a FBG due to a nonlinear strain profile along an FBG is through the use of the

transfer matrix method, where the FBG is split up into many small segments with constant properties. In this work, the modified transfer matrix formulation is used to account for the fact that high strain gradients are expected [52].

The transfer matrix of a single m_{th} section of the grating is given by

$$\boldsymbol{F_m} = \begin{bmatrix} \cosh(\Omega\Delta z) - j\frac{\xi}{\Omega}\sinh(\Omega\Delta z) & -j\frac{K}{\Omega}\sinh(\Omega\Delta z) \\ j\frac{K}{\Omega}\sinh(\Omega\Delta z) & \cosh(\Omega\Delta z) - j\frac{\xi}{\Omega}\sinh(\Omega\Delta z) \end{bmatrix}, \tag{3-2}$$

where Δz is the segment length, and

$$\boldsymbol{\Omega} = \sqrt{\boldsymbol{K^2 - \xi^2}}, \tag{3-3}$$

where K is the ac coupling coefficient and ξ is the dc self-coupling coefficient. The ac coupling coefficient is defined as

$$K = \frac{\pi}{\lambda} s\Delta n \boldsymbol{g(z)} \tag{3-4}$$

where s is the fringe visibility, and Δn is the refractive index contrast of the grating. $\boldsymbol{g(z)}$ is the change in the index contrast due to apodization during manufacturing, which is the deviation from a constant periodic structure along the FBG and is commonly assumed to be a Gaussian of the form

$$\boldsymbol{g(z)} = \exp\left(-\frac{4ln(2)\left(z-\frac{L}{2}\right)^2}{\rho^2}\right), \tag{3-5}$$

where ρ is the apodization constant, and L is the total length of the grating. The dc self-coupling coefficient is defined as

$$\xi = \frac{2\pi}{\lambda} n_e - \frac{\pi}{\Lambda}, \tag{3-6}$$

where λ is the free space wavelength, n_e is the effective refractive index of the optical fiber fundamental mode, and Λ is the effective grating period.

The grating period varies along the length of the grating with the applied strain $\boldsymbol{\varepsilon(z)}$ and the strain gradient $\boldsymbol{\varepsilon'(z)}$ as given by

$$\boldsymbol{\Lambda(z)} = \Lambda_0[1 + \boldsymbol{\varepsilon(z)} + z\boldsymbol{\varepsilon'(z)}]. \tag{3-7}$$

Similarly, the strain also creates a variation in n_e as given by

$$\boldsymbol{n_e(z)} = n_{e0} - p_e n_{e0}(\boldsymbol{\varepsilon(z)} + z\boldsymbol{\varepsilon'(z)}), \tag{3-8}$$

where p_e is the photoelastic constant of the FBG which for this work is 0.22 and n_{e0} is the effective refractive index before any strain is applied.

Defining F_m as the matrix of the m_{th} section of the grating, the matrix F for the combined grating is given by

$$\boldsymbol{F} = \begin{bmatrix} f_{11} & f_{12} \\ f_{21} & f_{22} \end{bmatrix} = \boldsymbol{F_m F_{m-1} \ldots . F_2 F_1}, \tag{3-9}$$

and from F the reflection coefficient of the FBG is given by

$$R = \left|\frac{f_{21}}{f_{11}}\right|^{\mathbf{2}}. \tag{3-10}$$

The optimization algorithm then computes the difference between the optimized and measured spectra as given by

$$f_{merit} = \sum_{j=1}^{s}[\boldsymbol{R_{opt,j}(\lambda_j)} - \boldsymbol{R_{meas,j}(\lambda_j)}]^2, \tag{3- 11}$$

where $\boldsymbol{R_{opt,j}(\lambda_j)}$ is the optimized FBG reflection spectrum and $\boldsymbol{R_{meas,j}(\lambda_j)}$ is the measured FBG reflection spectrum.

Figure 3-7 shows the block diagram for the algorithm to optimize an FBG spectrum to an unknown strain profile. An initial strain profile along the FBG is assumed which is used to generate a transfer matrix for the FBG, and therefore a predicted FBG spectrum. In this work, the built-in MATLAB optimization method fmincon is used [53].

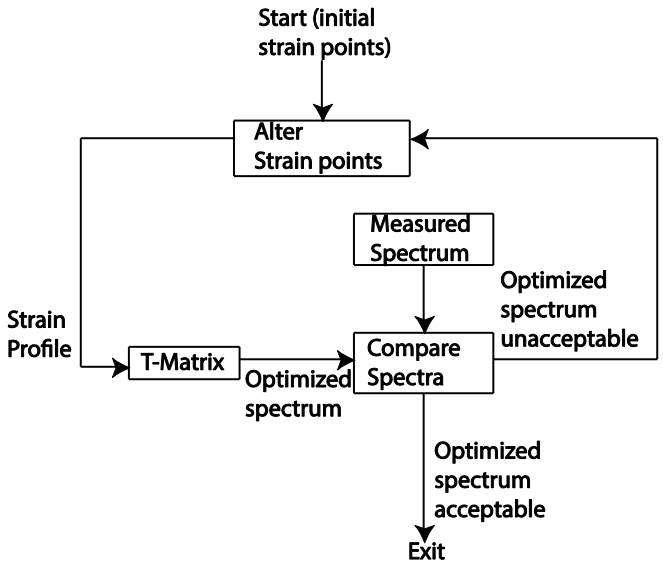

Figure 3-7: Optimization procedure for determining the strain gradient across the FBG. An initial assumption is made for a strain profile which is fed into the transfer matrix. The variance between the measured spectra and the simulated spectra are compared and the strain profile is altered until the variance is minimized.

If the difference between the two spectra is within a certain tolerance, then the optimization algorithm deems the optimized FBG strain profile as acceptable and returns. Otherwise, it repeatedly mutates the strain profile and continues to compare simulated and measured FBG spectra until the tolerance is reached. In this work, a maximum accepted average difference threshold of 0.00166 per data point was used.

3.4 Measurement Setup

In this work a split Hopkinson tensile bar is used to pull a specimen in tension [20][21][22][23]. Figure 3-8 shows an illustration of a split Hopkinson tensile bar that is capable of applying high tensile, compressive, or torsional strain rates (10^2 to 10^4 s^{-1}) depending on how the ends of the bars are displaced.

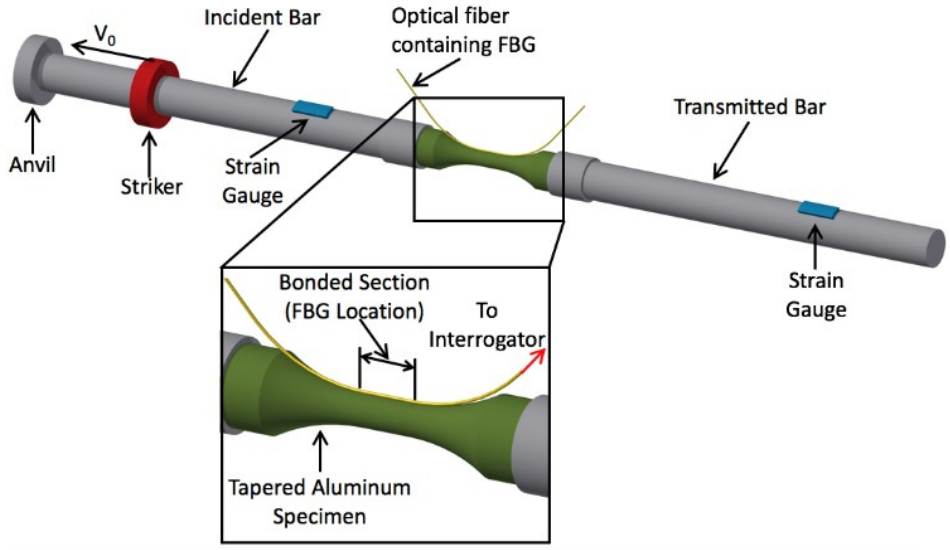

Figure 3-8. The split Hopkinson tensile bar consists of two bars holding a tapered specimen in the middle. Stress waves in the bars produce displacements in the specimen resulting in strain. The FBG is mounted across the tapered aluminum specimen to monitor the strain across the specimen over time.

The system works by firing the striker into the anvil at the end of the incident bar. This causes a compressive wave that is reflected back as a tensile wave when it reaches the end of the anvil. This tensile wave then travels all the way down the length of the incident bar. When it reaches the specimen some of the stress pulse is transmitted through the specimen and some is

reflected back based on the mismatch of the materials. The stress wave that goes into the specimen is then transmitted to the transmitted bar.

Both the incident and transmitted bars are made out of maraging steel while the specimen used was machined from 6061 aluminum to a gauged diameter of 0.51 cm and a gaged length of 2.5 cm. The bar used was a ¾ inch tensile bar, the striker was 12 inches long and the firing pressure was 30 psi.

Figure 3-8 shows that the FBG is glued onto the specimen along the length of the specimen, therefore measuring the strain on the surface of the specimen. In this work, a micron os1100 FBG is used with a theoretical strain limit of around 5 millistrain. The FBG was glued to the specimen using M-Bond AE-10 produced by Micro Measurements. M-Bond AE-10 is a room temperature cure two part epoxy capable of surviving up to 10% elongation.

3.5 Measurement Results

To verify the results found from the FBG interrogation, strains were also measured by electrical strain gauges on both the incident and transmitted bars. Additionally, a Photron Fastcam SA-X2 took high speed video of the specimen during the test. The Fastcam SA-X2 was set to take images at 100k frames per second, and VIC-2D software by Correlated Solutions was used to conduct the DIC analysis to measure the strain along the bar.

There is an estimated 5 μs time difference between the captured high speed video image frames and the FBG wavelength time frames. Figure 3-9 shows a screen capture from high speed video. The frame corresponds to 235 μs, which is close to FBG spectrum measured at 230 μs. Figure 3-9 also provides the DIC strain measurement.

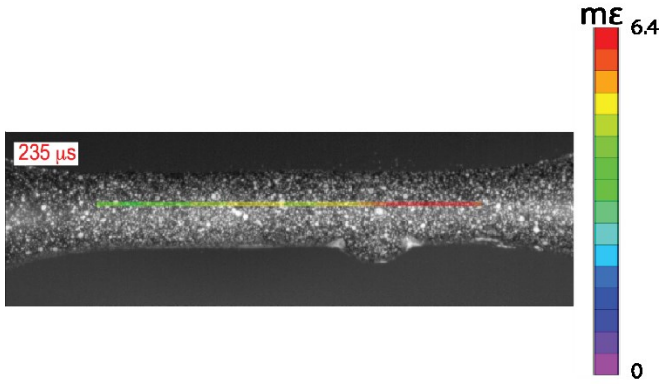

Figure 3-9: The DIC software allows for strain profile reconstruction by tracking a speckle pattern along the surface of the specimen. This strain profile was measured at 235 μs.

Figure 3-10 (solid) shows a line profile of the DIC strain measurement for the frame at time 235 μs along with (dashed) the FBG strain measurement corresponding to the time 230 μs. The optimization method described in Section 3.3 was used on the FBG spectra to determine the strain profile across the grating. To reduce the effects of the noise, a discrete cosine transform to represent 99% of the power from the data is applied [54]. Figure 3-10 shows that the new strain measurement based on high-speed FBG interrogation agrees well with the existing DIC measurement.

Figure 3-9 shows that the virtual DIC strain gauge is located in the center of the specimen for best tracking. The FBG is located directly at the top of the specimen, where DIC tracking would yield inaccurate data on a surface that is not directly facing the camera. The DIC virtual strain gauge also averages over 10 pixels, which would not allow it to measure very discrete changes in the strain profile along the specimen. This is a main advantage of using a high-speed full-spectrum FBG interrogator, in which a line of sight is not needed in order to deduce localized strain profiles.

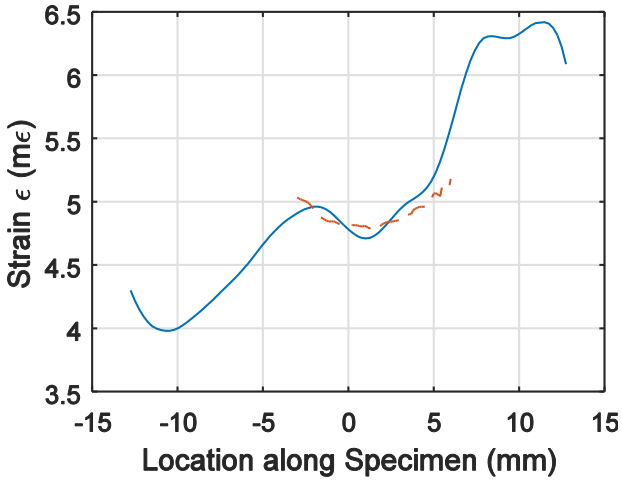

Figure 3-10: (solid blue line) Measured strain profile from DIC at 235 µs and (dashed red line) optimized strain profile for 230 µs. The strain profiles from the FBG and DIC agree with each other until the peak splitting phenomenon.

Figure 3-11 shows a false color image of the captured FBG wavelength spectra over time. The high-speed full-spectrum interrogator has a repetition rate of 100 kHz. This means that every 10 µs a new FBG reflection spectrum is measured. There are FBG spectra in which the shape stays approximately the same but is simply shifted in wavelength. This uniform shift corresponds to uniform strain across the grating. However, there are also regions in which the spectrum is distorted because of non-uniform strain. The average strain across the FBG can be determined by finding the centroid of each reflection peak and then multiplying it by the strain sensitivity of 1.2 pm/µε. This averaging approach is called peak tracking.

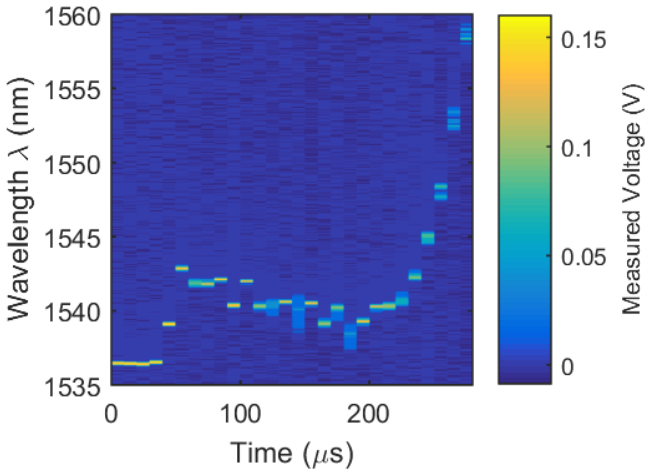

Figure 3-11: False color representation of captured FBG spectra over time. Full-spectrum high-speed interrogation allows the spectrum deformations to be captured. These deformations can later be analyzed to deduce the strain profile across the FBG.

Figure 3-12 shows the strain at the location of the FBG using three different measurement methods. These methods are (dot dashed black line) using peak tracking on the measured FBG spectrums, (solid red line) estimating the average strain using the electrical strain gauges placed on the transmitted and incident bars (see Figure 3-8), and (dashed blue line) using DIC average over the grating location. As can be seen, all three methods roughly agree on the strain profile over time.

The region in Figure 3-12 around 40 μs corresponds to the time when the tensile wave reaches the location of the FBG. Around 50 μs the sample reaches a local peak and something starts to slip and holds a constant load until 220 μs when the sample is loaded again. Figure 3-13 shows the strain rate from the three measurement methods. The overall trends illustrated by the graphs agree with each other.

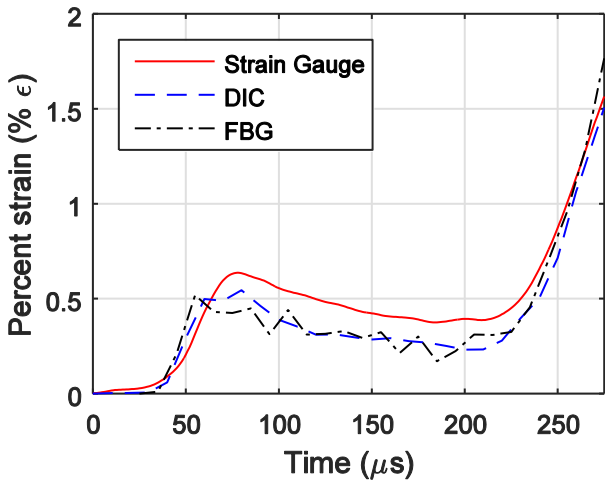

Figure 3-12: Measured percent strain on the FBG from the strain gauges (solid red line), DIC (dashed blue line) and FBG (dot dashed black line). The percent strain over time from the FBG agrees with the percent strain over time deduced by the DIC and strain gauges, this verifies that an FBG is a reliable tool for Hopkinson bar interrogation.

The high-speed full-spectrum interrogation method not only allows for the peak shift to be detected, but also allows for deformations in the FBG spectrum to be analyzed. These deformations need to be analyzed to understand strain profiles and strain gradients across the FBG, this was not possible with conventional peak tracking.

During the first 50 μs the FBG spectra stays approximately uniform. Between 50 μs and 200 μs some spectra are uniform while others are distorted. After the reflected tensile wave reaches the FBG around the time of 200 μs the spectra remain distorted.

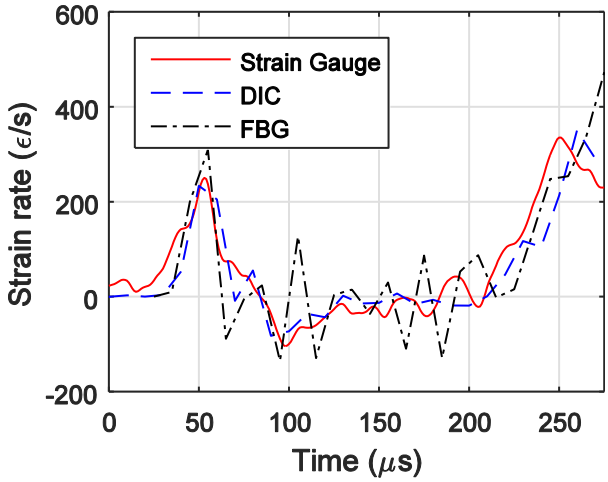

Figure 3-13: Measured average strain rate from the FBG using peak detection on the measured spectra: strain gauges (solid red line), DIC (dashed blue line) and FBG (dot dashed black line). The highest strain rate achieved is approximately 500 s^{-1}.

Figure 3-14 shows five of the FBG spectra from time 210 μs to 250 μs. The right side of Figure 3-14 shows the calculated strain profiles. Using the FBG strain measurement conclusions about the cause of the failure point can be deduced. For example, at 4 mm along the grating length a discrete change in the strain occurs. It is assumed that this discrete change in the strain causes a break in the optical fiber. The exact cause of the discrete jump in strain is unknown. However, it could be part of the glue breaking off of the aluminum bar resulting in different strain values on the two halves of the grating [55].

Figure 3-15 (top) shows the screen capture from 245 μs where a crack was first detected by the FBG and Figure 3-15 (middle) shows a break point on the glue that can be seen at 305 μs on the high speed camera video frames. Figure 3-15 also shows that the assumed FBG location overlaps the section where the glue broke off, which creates a discrete jump in the strain profile and peak splitting as is seen in Figure 3-14.

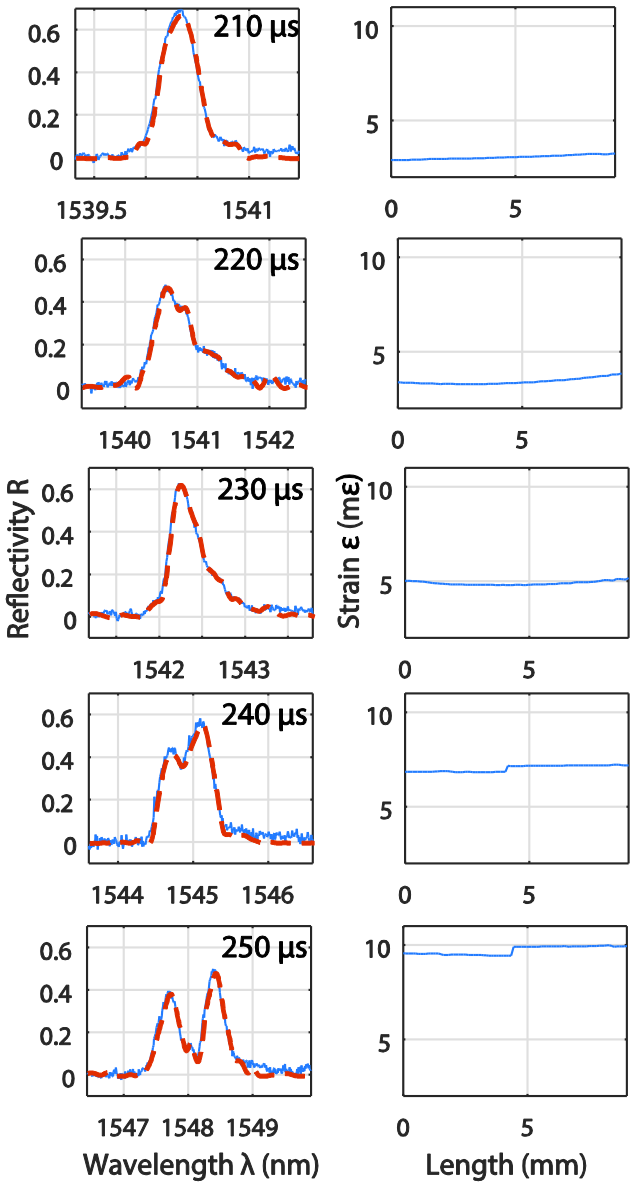

Figure 3-14: The left column shows (solid blue line) the measured spectrums and (dashed red line) the optimized spectrums over 10 µs intervals. The right column shows the optimized strain profiles. The strain discontinuities shown at 240 µs and 250 µs indicate localized material failure which is important in material analysis.

The fiber doesn't separate from the specimen until a few stress pulses later at around 1350 µs. Figure 3-15 (bottom) shows the fiber separation from the specimen at 1395 µs where the broken fiber ends can be seen. It is assumed that the sharp strain gradient is what caused the break in the fiber at the FBG location.

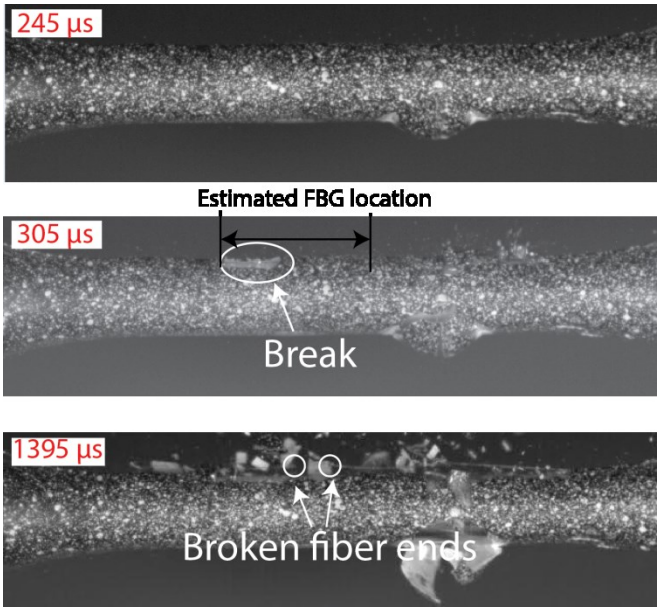

Figure 3-15: (top) High speed camera image corresponding to 240 µs from the FBG measurement where a crack is first detected by the FBG, and (middle) high speed camera image corresponding to 305 µs where the crack first manifests itself from the high speed camera video images. (bottom) The broken fiber ends can be seen at 1395 µs on the high speed camera video images.

The FBG is able to detect localized strain discontinuities at the moment of the event without a direct line of sight. The FBG used in this work was surface mounted to the specimen, but it has been shown that FBGs can be embedded inside Hopkinson bar specimen [13]. This would allow for a direct internal strain profile analysis over time on the specimen during a Hopkinson bar test or any other high speed event.

3.6 Summary

This work presents a method for analyzing dynamic, localized strain distributions through the use of a single FBG sensor. By using a swept laser source with a sweep repetition rate of 100

kHz, the entire deformation of the FBG spectrum can be captured to analyze strain gradients across the material as a function of position and time. A tensile Hopkinson bar specimen produced strain rates up to 500 s^{-1} and DIC measurements were used to validate the accuracy of the FBG measurements.

The transfer matrix optimization method is used on the deformed spectrum of the FBG. It is possible to deduce the strain gradient across the FBG, and predict where a specimen will fail or tell where a specimen has failed. This method does not require a full view of the specimen or strain gauges.

The FBG used in this work was surface mounted to the Hopkinson bar specimen, however, FBG's offer the ability to be both surface mounted or embedded allowing for strain profile analysis without a direct line of sight during high speed events.

4 CONCLUSION

This thesis shows improvements to 2 different fiber optic sensors which make them more applicable and feasible. Specifically, this thesis shows that through the push-pull configuration, that a SCOS is able to subtract out localized strain noise, and when coupled with external phase modulation, the SCOS is able to measure electric fields in a harsh environment by subtracting out all three noise sources.

This thesis also shows that through high-speed full-spectrum interrogation of FBGs, nonlinearities that arise from strain gradients can be deduced from FBGs. This is useful in applications such as Hopkinson bar measurements because this allows for internal strain gradients to be deduced without a direct line of sight.

4.1 Contributions

As mentioned in the introduction, the main contributions in this work are outlined as follows:

1. I developed an interrogation method to reduce 3 separate noise sources simultaneously in a SCOS in a harsh environment.
   (F. Seng, N. Stan, R. King, C. Josephson, L. Shumway, A.Hammond, and S. Schultz. "Optical sensing of Electric Fields in Harsh Environments." *Journal of Lightwave Technology,* under review.)

2. I developed a new SCOS prototype which is capable of handling localized vibration noise (F. Seng, N. Stan, C. Josephson, R. King, L. Shumway, R. Selfridge, S. Schultz. “Push-pull slab coupled optical sensor for measuring electric fields in a vibrational environment.” Applied Optics 54.16 (2015): 5203-09.)
3. I developed a high-speed full-spectrum interrogation system and used it on a Hopkinson bar impact.
   (F. Seng, D. Hackney, T. Goode, L. Shumway, A. Hammond, G. Shoemaker, M. Pankow, K. Peters, and S. Schultz. "Split-Hopkinson Bar Measurement Using High-Speed Full-Spectrum Fiber Bragg Grating Interrogation." *Applied Optics,* Accepted.)

4.2 Push-Pull SCOS

Research towards making SCOS that are vibration insensitive has been ongoing for over 5 years at the BYU electro optics lab. The research in this thesis has shown that a variant of the SCOS called the push-pull SCOS can handle localized noise due to high vibrations. This is done by adhering 2 lithium niobate crystals to the same D-fiber with their optic axes flipped opposite to each other. By doing this, the two SCOS sensing elements will have the same response to electric field but opposite response to strain. This allows for the strain noise to be subtracted out and the electric field signal to be recovered significantly.

4.3 High-Speed Full-Spectrum Interrogation of FBGs

Research towards high-speed full-spectrum interrogation on FBGs has been done before, but not with commercially available equipment. This thesis proves that high-speed full-spectrum interrogation can work for strain rates up to 500 s^{-1}, and that nonlinear strain gradients across the Hopkinson bar can be deduced without a direct line of sight.

4.4 Electric Field Sensing in Harsh Environments

When the push-pull is paired with external phase modulation, it is possible for the SCOS to optically measure electric fields in harsh environments by reducing three noise sources simultaneously. The three noise sources that are reduced are non-localized strain noise which manifests itself as interferometric noise, localized. The push-pull SCOS is unable to perform properly under circumstances where interferometric noise is present. Therefore the interferometric noise must first be up-converted and filtered out before the push-pull is used in a truly harsh environment.

4.5 Future Work

This thesis explores techniques for improving SCOS technology by decreasing three different noise types simultaneously. This thesis also validates the technique for high-speed full-spectrum FBG interrogation through high-speed full-spectrum interrogation of an FBG on a Hopkinson bar.

Although this thesis shows that noise sources have been decreased dramatically for a SCOS, work still needs to be done to increase the sensitivity of a SCOS to measure low electric fields in or outside of a harsh environment. Currently a visible signal from the SCOS in the time domain is on the order of kV/m. One potential method of overcoming this difficulty is through the use of a dipole antenna. Dipole antennas generate an amplified version of the applied electric field across the dipole gap.

Although this thesis shows that high-speed full-spectrum interrogation of FBGs is very effective in measuring strain gradients and large spectrum shifts, it is difficult to detect large shifts resulting from multiple FBGs that could lead to peak crossing. When multiple FBG peaks

cross and come out from crossing it is difficult for an algorithm to determine which FBG peak is which, therefore large errors could accumulate from such an event.

Finally, the SCOS is a good electric field sensor, but its sensitivity is generally not tunable as a fabrication process. It has been shown that gratings can be written into an electro optic waveguide, and that the peak shift can be monitored to deduce an electric field applied across the electro-optic material.

4.5.1 Dipole Antennas

Many modern day EO sensors such as Mach Zehnders rely on having a dipole antenna to help increase sensitivity. These dipole antennas are generally integrated into the sensor by printing them onto the substrate. These dipole antennas are typically used to generate an electric field local to the SCOS which is an amplified version of the field applied across the EO sensor, and experiments have shown dipole antennas to enhance the sensitivity of a SCOS by up to 30 times.

Dipole antennas can also be used to flip the directional sensitivity of the SCOS by 90 degrees. This is done with the configuration shown in Figure 4-1, where the dipole antenna length is perpendicular to the direction of its cap. This is because the field in the direction of the length of the dipole is amplified across the gap in the direction of the optic axis of the lithium niobate crystal, which is the most sensitive direction of the crystal. This not only flips the directional sensitivity of the SCOS by 90 degrees, but also enhances it by 2 times.

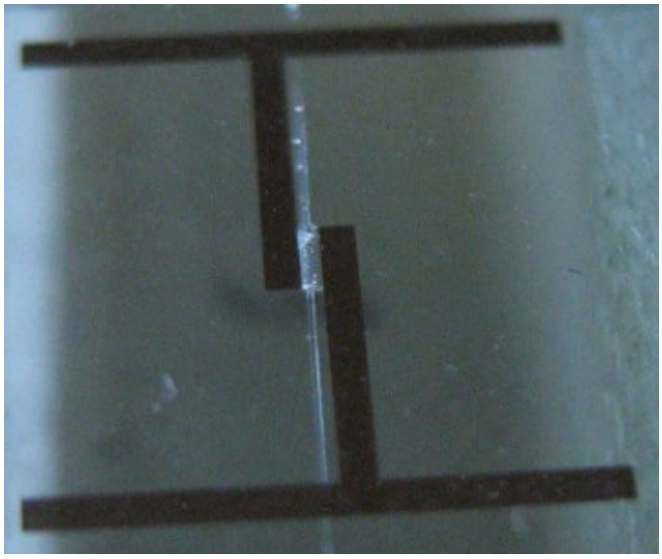

Figure 4-1. A cross dipole antenna can flip the directional sensitivity of the SCOS by amplifying a field along the fiber into the direction of the optic axis of the lithium niobate crystal.

4.5.2 Recursive Ransac Peak Tracking

Due to the recent progress of full spectrum tracking of FBGs, peak tracking is an area that has yet to be developed, especially when multiple FBG peaks cross over each other. Generally this is done by optimization for a whole sensor network, but due to the speed of optimization which could take up to tens of minutes per frame, this method is prohibitive for many applications. However, peak tracking is a problem that already has a solution since peak tracking is synonymous with target tracking. Unmanned vehicle research groups have researched target tracking for many years and have come up with a number of algorithms to track through swarms of UAVs.

One example of such an algorithm that has been developed at the BYU MAGIC lab is the recursive ransac algorithm, which is capable of tracking swarms of UAVS real time. By implementing the physical model of the recursive ransac algorithm which takes into account he velocities and accelerations of the UAVs, the velocities and the accelerations of the FBG can be

taken into account and multiple FBG peaks can be tracked through peak crossing. The speed up is considerable, reducing computation time from hours to seconds.

4.5.3 Electro-Optic Gratings Written into Electro-Optic Waveguide

A main cause for a peak shift in an FBG is the change of index in the optical fiber due to the photoelastic effect. However, a change in index in a material doesn't necessarily arise simply due to the photoelastic effect. For example in SCOS is arises due to the electro optic effect. This electro optic effect has been shown to be able to shift the peaks of a grating written into an electro optic material. Due to the maturity of grating technology, this would allow for the sensor's sensitivity to be tuned during fabrication.

It has been shown that Vernier gratings written in standard optical fiber offer very high sensitivity when interrogated using edge interrogation. Vernier gratings written into an electro optic waveguide would allow for the sensitivity of the electric field sensor to be tuned during fabrication based off of the Vernier design. This has a high potential to be a very sensitive electro optic sensor or even a modulator.

REFERENCES

[1] N. Stan, F. Seng, L. Shumway, R. King, R.H. Selfridge, and S.M. Schultz, "High electric field measurement using slab-coupled optical sensors," Appl. Opt. **55**, 603-610 (2016)

[2] C.Y Lin, A.X. Wang, B.S. Lee, X.Y. Zhang, and R.T. Chen, "High dynamic range electric field sensor for electromagnetic pulse detection," Opt. Express **19**, 17372-17377 (2011)

[3] E.K. Johnson, J.M. Kvavle, R.H. Selfridge, S.M. Schultz, R. Forber, W. Wang, and D.Y. Zang, "Electric field sensing with a hybrid polymer/glass fiber," Appl. Opt. **46**, 6953-6958 (2007)

[4] F. Seng, N. Stan, R. King, R. Worthen, L. Shumway, R.H. Selfridge, and S.M. Schultz, "Optical Sensing of Electrical Fields in Harsh Environments," in *Optical Fiber Communication Conference*, OSA Technical Digest (online) (Optical Society of America, 2016), paper M2D.3.

[5] J.R. Noren, "Electric Field Sensing in a Railgun Using Slab Coupled Optical Fiber Sensors" (2012). *All Theses and Dissertations.* Paper 3482. http://scholarsarchive.byu.edu/etd/3482

[6] R.B. Hoffman, T.L. Haran, and S.R. Lane. "Diagnostic capabilities for electromagnetic railguns." *Electromagnetic Launch Technology (EML), 2012 16th International Symposium on* (2012)

[7] B. Fryskowski. "Development of vacuum-tube-based voltage and current probes for automotive ignition systems."*Proceedings of the Institution of Mechanical Engineers, Part D: Journal of Automobile Engineering* 229.8 (2015): 958-68.

[8] B. Hnatiuc, D Astanei, S Pellerin, N Cerqueira, and M Hnatiuc. "Diagnostic of Plasma Produced by a Spark Plug at Atmospheric Pressure: Reduced Electric Field and Vibrational Temperature." *Contributions to Plasma Physics* 54.8 (2014): 712-23.

[9] S.J. Mihailov, Fiber Bragg Grating Sensors for Harsh Environments. *Sensors* **2012**, *12*, 1898-1918.

[10] H. Dong, W. Zhao, T. Sun, K.T.V. Grattan, A I. Dong, C. Al-Shamma'A, J. Wei, J. Mulrooney, C. Clifford, E. Fitzpatrick, M. Lewis, H. Degner, S.I. Ewald, G. Lochmann, E. Bramann, P. Merlone Borla, M. Faraldi, and M. Pidria. "Vibration-insensitive temperature sensing system based on fluorescence decay and using a digital processing approach." *Measurement Science and Technology* 17.7 (2006).

[11] K. Bohnert, P. Gabius, J. Nehring, and H. Brandle. "Temperature and Vibration Insensitive Fiber-Optic Current Sensor." *Journal Of Lightwave Technology* 20.2 (2002).

[12] R. Gibson, R.Selfridge, S.Schultz, W. Wang, and R. Forber. "Electro-optic sensor from high Q resonance between optical D-fiber and slab waveguide." *Applied Optics* 47.13 (2008): 3505-12.

[13] W. Lin, L. Tsai, C. Chiang, and S. Wang. "High strain rate characteristics of fiber Bragg grating strain sensors." Proceedings of the SEM International Conference and Exposition on Experimental and Applied Mechanics(2012)

[14] J. Ayers, T. Weerasooriya, A. Ghoshal, C. Pecora, and A. Gunnarsson. "Feasibility of structural health monitoring of high strain rate events using fiber Bragg grating sensors." Proceedings of the ASME 2012 Conference on Smart Materials, Adaptive Structures and Intelligent Systems SMASIS2012 (2012).

[15] D. Kinet, P. Mégret, K.W. Goossen, L. Qiu, D. Heider, C. Caucheteur. “Fiber Bragg grating sensors toward structural health monitoring in composite materials: challenges and solutions.” *Sensors 14 (*2014): 7394-7419.

[16] A. Gill, K. Peters, and M. Studer. "Genetic algorithm for the reconstruction of Bragg grating sensor strain profiles." Measurement Science and Technology 15.9 (2004): 1877-84.

[17] X. Wen, and Q. Yu. "Reconstruction of strain distribution in fiber Bragg gratings with differential evolution algorithm." Optoelectronics Letters 4.6 (2008): 403-06.

[18] D.H. Kang, S.O Park, C.S. Hong, and C.G. Kim. "The signal characteristics of reflected spectra of fiber Bragg grating sensors with strain gradients and grating lengths." NDT & E International 38.8 (2005): 712-18.

[19] S. Chadderdon, T. Vella, R.H.Selfridge, S.M. Schultz, S. Webb, C. Park, K. Peters, and M. Zikry. "High-speed full-spectrum interrogation of fiber Bragg gratings for composite impact sensing." Proc. SPIE 7648, Smart Sensor Phenomena, Technology, Networks, and Systems 2010, (2010).

[20] K. Xia, and W. Yao. "Dynamic rock tests using split Hopkinson (Kolsky) bar system - A review." Journal of Rock Mechanics and Geotechnical Engineering 7.1 (2015): 27-59.

[21] J.T. Foster. "Comments on the validity of test conditions for kolsky bar testing of elastic-brittle materials." Experimental Mechanics 52.9 (2012): 1559-63.

[22] W.N Sharpe. Springer Handbook of Experimental Solid Mechanics. Boston: Springer, 2008. 929-30.

[23] W.W. Chen and B. Song. Split Hopkinson (Kolsky) Bar. Springer, 2011.

[24] A. Bandhyopadhya, and S. Bose. Characterization of Biomaterials. Oxford: Elsevier, 2013. 95.

[25] W. Zhou, J. Zhao, Y. Liu, and Q. Yang. "Simulation of localization failure with strain-gradient-enhanced damage mechanics." International Journal for Numerical and Analytical Methods in Geomechanics 26.8 (2002): 793-813.

[26] J. Li, T. Pham, R. Abdelmoula, F. Song, and C.P. Jiang. "A micromechanics-based strain gradient damage model for fracture prediction of brittle materials – Part II: Damage modeling and numerical simulations." International Journal of Solids and Structures 48.24 (2011): 3346-58.

[27] F. Seng, N. Stan, C. Josephson, R. King, L. Shumway, R. Selfridge, and S. Schultz, "Push–pull slab coupled optical sensor for measuring electric fields in a vibrational environment," Appl. Opt. 54, 5203-5209 (2015)

[28] J. Cole, C. Kirkendall, and A. Dandridge. "Fiber optic acoustic sensor technology." *The Journal of the Acoustical Society of America* 117 (2005).

[29] W. H. Steier, "A push-pull optical amplitude modulator." *Quantum Electronics, IEEE Journal of* 3.12 (1967).

[30] X. Zhang, D.F. Xue, and K. Kitamura. "Domain characteristics and chemical bonds of lithium niobate." *Materials Science and Engineering B* 120.1-3 (2005).

[31] J.H. Hines, D.C. Malocha, K.B. Sundaram, K.J. Casey, and K.R. Lee. "Deposition parameter studies and surface acoustic wave characterization of PECVD silicon nitride films on lithium niobate." *IEEE Transactions on Ultrasonics, Ferroelectrics and Frequency Control* 42.3 (1995).

[32] H.S. Jung,. "Electro-optic Electric Field Sensor Utilizing Ti:LiNbO3 Symmetric Mach-Zehnder Interferometers." *Journal of the Optical Society of Korea* 16.1 (2012).

[33] A. Garzarella,, D.H. Wu, and R J. Hinton. "Progress in High Sensitivity Electro-optic Field Sensors." *Lasers and Electro-Optics, 2007. CLEO 2007. Conference on* (2007).

[34] R. Zeng, W.Y. Chen, J.L. He, and P. Zhu. "The Development of Integrated Electro-optic Sensor for Intensive Electric Field Measurement." *Electromagnetic Compatibility, 2007. EMC 2007. IEEE International Symposium on* (2007).

[35] W. Jin, Y. Z. Xu, M. S. Demokan, and G. Stewart, "Investigation of interferometric noise in fiber-optic gas sensors with use of wavelength modulation spectroscopy," Appl. Opt. 36, 7239-7246 (1997)

[36] W. Jin. "Investigation of interferometric noise in fiber-optic Bragg grating sensors by use of tunable laser sources." Applied Optics 37.13 (1998).

[37] P.K. Pepeljugoski, and K.Y. Lau. "Interferometric Noise Reduction in Fiber-Optic Links by Superposition of High Frequency Modulation." Journal Of Lightwave Technology 10.7 (1992).

[38] E.H. Chan, "Suppression of phase-induced intensity noise in fibre optic delay line signal processors using an optical phase modulation technique." Optics Express 18.21 (2010).

[39] L. Couch, W. *Digital and Analog Communication Systems*. 6th ed. Upper Saddle River: Prentice Hall Inc., 2001. 318-22.

[40] B.E.A. Saleh, and M.C. Teich. *Fundamentals of Photonics*. 2nd ed. Hoboken: John Wiley and Sons, 2007. 836-39.

[41] “Thorlabs LN53S-FC-10GHz Phase Modulator data sheet.” *Thorlabs*.

[42] R.E. Ziemer, “Principles of communications." (1976)

[43] M. Tur, and E.L. Goldstein. "Probability distribution of phase-induced intensity noise generated by distributed-feedback lasers." *Optics Letters* 15.1 (1989): 1-3.

[44] N. Stan, Bailey D., Chadderdon S., Webb S., Zikry M., Peters K., Selfridge R., and Schultz S., "Increasing dynamic range of a fibre Bragg grating edge-filtering interrogator with a proportional control loop," Measurement Science and Technology, 25, 1-8 (2014).

[45] R. Romero, O. Frazao, P.V.S. Marques, H.M. Salgado, and J.L. Santos. "Fibre Bragg grating interrogation technique based on a chirped grating written in an erbium-doped fibre." *Measurement Science & Technology* 14.11 (2003): 1993-97.

[46] U. Tiwari, K. Thyagarajan, M.R. Shenoy, and S.C. Jain. "EDF-Based Edge-Filter Interrogation Scheme for FBG Sensors." *Sensors Journal, IEEE* 13.4 (2012): 1315-19.

[47] R.R. Burgett, R.E. Massoll, and D.R. Van Uum. "Relationship between Spark Plugs and Engine-Radiated Electromagnetic Interference." *IEEE Transactions on Electromagnetic Compatibility* EMC-16.3 (1974): 160-72.

[48] F. Canavero, E. Cardelli, M. Raugi, and A. Tellini. "Modelling of Electromagnetic Interferences produced by a Railgun." *IEEE Transactions on Magnetics* 29.1 (1993): 1125-30.

[49] H. Bluhm. *Pulsed Power Systems, Principles and Applications*. Springer-Verlag Berlin Heidelberg, 2006. 211.

[50] "Fiber Bragg Grating os 1100 datasheet." Micron Optics.

[51] M. Bonesi, M.P. Minneman, J. Ensher, B. Zabihain, H. Sattmann, P. Boschert, R.A. Leitgeb, M. Crawford, W. Drexler. "Akinetic all-semiconductor programmable swept-source at 1550 nm and 1310 nm with centimeters coherence length." Optics Express 22.3 (2014): 2632-55.

[52] M. Prabhugoud, and K. Peters. "Modified transfer matrix formulation for Bragg grating strain sensors." Journal of Lightwave Technology 22.10 (2004): 2302-09.

[53] A. Karageorghis, D. Lesnic, and L. Martin. "The method of fundamental solutions for solving direct and inverse Signorini problems." Computers and Structures 151 (2015): 11-19.

[54] L. Thévenaz and M. A. Soto, "Novel concepts and recent progress in distributed optical fiber sensing," *Optical Fiber Communication Conference*, OSA Technical Digest (online) (Optical Society of America, 2016), paper M2D.5.

[55] G.F. Pereira, L.P. Mikkelsen, and M. McGugan. "Monitoring of fatigue crack growth in composite adhesively bonded joints using Fiber Bragg Gratings." Proceedings of the 5th International Conference on Smart Materials and Nanotechnology in Engineering (SMN) in conjunction with the International Conference on Smart Materials and Structures (Cansmart 2015) (2015).

5 APPENDIX

5.1 Silicon Nitride Deposition on lithium niobate crystal

1. Dehydration bake wafer.
2. Adhere lithium niobate crystal onto wafer using MY-145 UV adhesive.
3. Keep UV light on for 10 minutes to ensure full UV adhesive cure.
4. Bake wafer at 250 degrees celcius for 10 minutes to ensure all moisture from UV adhesive is gone.
5. Instructions for deposition for silicon nitride using the PECVD machine are listed on the BYU cleanroom website.
6. Deposit 200 nm of silicon nitride for 3 nm shift.
7. Soak wafer with acetone to remove lithium niobate crystal. Usually soaking overnight is sufficient.

5.2 MATLAB Slicing Code

This is the code that reads in the three waveforms from the high-speed full-spectrum interrogator, specifically, the start sweep/end sweep waveform, the FBG signal waveform, and the data valid vector. This algorithm then takes chunks of the FBG signal waveform and the data valid waveform corresponding to single sweeps and organizes individual sweeps into individual rows in two matrices. It then outputs the two matrices into dat files, which are then fed into an error correction MATLAB code

```
close all
clear all

% read in files
%%%%%%%%%%%%%%%%%%%%%%%%%%%%%%%% option for LeCroy waveform%%%%%%%%%%%%%%%%
info1 = ReadLeCroyBinaryWaveform('C1mqrimbahi00000.trc'); %start sweep file
t = info1.x;
V = info1.y;

info1 = ReadLeCroyBinaryWaveform('C2mqrimbahi00000.trc');%error file
t1 = info1.x;
V1 = info1.y;

info1 = ReadLeCroyBinaryWaveform('C3mqrimbahi00000.trc');%reading file
t2 = info1.x;
V2 = info1.y;

%% %%%%%%%%%%%%%%%%%%%%%%%%%%%%%%%%%%%%%%%%%%%%%%%%%%%%%%%%option for csv files%%%%%%%%%%%%%%%

% info1 = csvread('scope_8.csv',3,0); %start sweep signal
% t= info1(:,1);
% V=info1(:,3);
% t2=info1(:,1);
% V2=info1(:,2);
%
% info1 = csvread('nameofdatafile',2,0); %error line
% t1= info1(:,1);
% V1=info1(:,2);

%
% info1 = csvread('nameofdatafile',2,0); %grating spectrum capture line
% t2= info1(:,1);
% V2=info1(:,2);

%%%%%%%%%%%%%%%%%%%%%%%%%%%% option for agilent binary files%%%%%%%%%%%%%%%%%%%%%%
%binary files you need to save one channel at a time.
% [t,V] = importAgilentBin('scope_16.bin'); %start sweep signal
% [t1,V1] = importAgilentBin('scope_18.bin');%data valid waveform
% [t2,V2] = importAgilentBin('scope_17.bin');%waveform

%%

    % we first break up everything and load them into a 2x 2 array
    ii=1;
```

```
    jj=0; %this will be the number for counting the number of sample points
in one time frame.

    startnewsweep=0;
    timeholder=zeros(2,2);
    timeholderrow=1; %start off on the first row of the timeholder matrix
    startingclock=V(1,1);
    updownboolean=0;

    %the updown boolean will help us determine what the next threshold we
    %should look for is. i.e. should we look for an edge that is greater
    %than or less than?

    if(startingclock<1.500)
        updownboolean=0;% this is if we are starting on the low clock edge
    else
        updownboolean=1;%this is if we are starting on the high clock edge
    end
    endpoint=size(t);

    gettimeperiod=0; %to match time to wavelength, we need to know the sweeep
time

    %go through all the points

    timeperiodstart=0;
    timeperiodend=0;

    h = waitbar(0,'Please wait...');
    %go through all the points
    while gettimeperiod<2
        %while we have not hit a threshold condition keep appending points
        %to the current location in the 2D matrix.
        timeholdercolumn=1; %start off on the first column on the timeholder
column
        startnewsweep=0;

        while (startnewsweep < 0.5) && (ii < endpoint(1,1))
           timeholder(timeholderrow,timeholdercolumn)=V2(ii);

            ii=ii+1;

             if(updownboolean==0 && V(ii)>1.500)
                updownboolean=1;
                startnewsweep=1;

                if(gettimeperiod==0) %we are ready to start seeing what the
time period is
                    gettimeperiod=1;
                    timeperiodstart =t(ii);
                else
                    if gettimeperiod==1 %otherwise we want to see what the
end of the time period is
```

```
                    timeperiodend=t(ii);
                    gettimeperiod=2;
                end
            end


        else
            if(updownboolean==1 && V(ii)<1.500)
                updownboolean=0;
                 startnewsweep=1;

            if(gettimeperiod==0) %we are ready to start seeing what the
time period is
                gettimeperiod=1;
                timeperiodstart =t(ii);
            else
                if gettimeperiod==1 %otherwise we want to see what the
end of the time period is
                    timeperiodend=t(ii);
                    gettimeperiod=2;
                end
            end
             end
        end

        if gettimeperiod==1
           jj=jj+1;
        end


        if(V(ii)>1.500)
            V(ii);
        end
        timeholdercolumn=timeholdercolumn+1;


        waitbar(ii / endpoint(1,1))
    end
    n=1;
    timeholderrow=timeholderrow+1;
    gettimeperiod
 end

  jj=jj
 timeholderpermenant=zeros(round(endpoint(1,1)/jj),(jj)+1);
 errorholderpermenant=zeros(round(endpoint(1,1)/jj),(jj)+1);
 alternator=0;
 temp=zeros(1,1);
 timeholderrow=1;
offsetter=1
if(V(1:ii)<1.500)
    updownboolean=0;% this is if we are starting on the low clock edge
 else
    updownboolean=1;%this is if we are starting on the high clock edge
end
```

```
    % these figures give us an initial look at our data
    figure(100)
    plot(t(1:ii),V(1:ii))

    figure(101)
    plot(t,V,t2,V2);

    %saveas(h0, 'oneontopofother','fig');

    correctionperiod=1;
    numberofcorrections=0;
     while ii<(endpoint(1,1)-jj*2)
         % we have to take care of an inconsistant sample time with the
         % clock
         if(updownboolean==1) % if we are on a high clock edge, then we should
be on a low clock edge, so increase our point until we hit the low clock edge
             if(V(ii+jj,1)>1.500)
                 while V(ii+jj,1)>1.500
                     ii=ii+1;
                     numberofcorrections=numberofcorrections+1;
                 end
                 updownboolean=0;
                 temp=V2(ii:(ii+jj),1);
                 size(temp)
                 errortemp=V1(ii:(ii+jj),1);
                 errorholderpermenant(timeholderrow,:)=transpose(errortemp);
                 timeholderpermenant(timeholderrow,:)=transpose(temp);
             else
                 while V(ii+jj,1)<1.500 %otherwise if we're on the low clock
edge, decrease our point until we hit the high clock edge
                     ii=ii-1;
                     numberofcorrections=numberofcorrections+1;
                 end
                 updownboolean=0;
                 temp=V2(ii:(ii+jj),1);
                 size(temp)
                 errortemp=V1(ii:(ii+jj),1);
                 errorholderpermenant(timeholderrow,:)=transpose(errortemp);
                 timeholderpermenant(timeholderrow,:)=transpose(temp);
             end
         else if (updownboolean==0)  % if we are on a low clock edge, if we
see that we are on a high clock edge, decrease our point until we hit the low
clock edge
                 if(V(ii+jj,1)>1.500)
                     while V(ii+jj,1)>1.500
                         ii=ii-1;
                         numberofcorrections=numberofcorrections+1;
                     end
                     updownboolean=1;
                     temp=V2(ii:(ii+jj),1);
                     size(temp)
                                     errortemp=V1(ii:(ii+jj),1);
                 errorholderpermenant(timeholderrow,:)=transpose(errortemp);
                     timeholderpermenant(timeholderrow,:)=transpose(temp);
```

```
                else  %otherwise increase our point until we hit a high clock
edge
                    while V(ii+jj,1)<1.500
                        ii=ii+1;
                        n=0;
                        numberofcorrections=numberofcorrections+1;
                    end
                    updownboolean=1;
                    temp=V2(ii:(ii+jj),1);
                    size(temp)
                                    errortemp=V1(ii:(ii+jj),1);
                errorholderpermenant(timeholderrow,:)=transpose(errortemp);
                    timeholderpermenant(timeholderrow,:)=transpose(temp);
                end
            end
        end
        ii=ii+jj;
        timeholderrow=timeholderrow+1;
        waitbar(ii / endpoint(1,1))

    end

    close(h)
 %write the sliced waveform file and the sliced error file
    csvwrite('30cmC400002.dat',timeholderpermenant);
    csvwrite('30cmC4error00002.dat',errorholderpermenant);
```

5.3 MATLAB Error Correction Code

This is the code that takes in the FBG waveform matrix and the data valid matrix from the slicing code and removes the data invalid points from the FBG waveform matrix. This is done by taking the 0s in the data valid vector as data invalid points removing points from the FBG waveform matrix with the same position. The points in the FBG waveform matrix that correspond to the 1s positions in data valid vector are kept.

```
close all
clear all

%read in the waveform and error file from manualrun
segmentdata=csvread('impacttimedata636465.dat');
errordata=csvread('impacterrordat636465.dat');

%sweep parameters, once again we will not use these in this code
sizeofdata=size(segmentdata);
c=3*10^8;
minwavelength=1534.22;
maxwavelength=1564.59;
timeperiod=9.4100e-06;
minfreq=c/(minwavelength*10^(-9));
maxfreq=c/(maxwavelength*10^(-9));
fnew=linspace(minfreq,maxfreq,sizeofdata(1,2));
lambdanew=c./(fnew);
time=sizeofdata(1,1).*timeperiod;
timenew=linspace(0,sizeofdata(1,1)*timeperiod,sizeofdata(1,1));
datapoints=linspace(0,sizeofdata(1,1),sizeofdata(1,1));

%start with one file, correct its error and see if it works, do this by
%finding where the first threshold is less than 1.5, and then finding the
%next threshold where we are greater than 1.5 interpolate the data between
%these points using pchip, and then replace the data with the pchip data.

ii=1
jj=0
timeholdernew = zeros(0,0);

h = waitbar(0,'Please wait...');

while ii<=sizeofdata(1,1)
    jj=1;
    while jj<=sizeofdata(1,2)
        if(errordata(ii,jj)<1.5)
            fixed=0;
            numberofpointstointerpolate=0;
            %take the starting point for the buffer value insert
            interpolatestart=segmentdata(ii,jj);
            %where to start replacement in original data
            if(jj>1)
                replacestartpoint=jj;
            else
                replacestartpoint=jj;
            end
```

```
            %find the ending point for the buffer value insert as well as
            %the number of points you need  to make it work
            while errordata(ii,jj)<1.5
                numberofpointstointerpolate=numberofpointstointerpolate+1;
                jj=jj+1;
                if(jj==sizeofdata(1,2))
                    break;
                end
            end
            %take the ending point for the buffer value insert

            interpolateend=segmentdata(ii,jj);
            %where to end buffer value insert in original data
            replaceendpoint=jj;
            x=1:2;
            y=[interpolatestart interpolateend];

            xx=linspace(1,numberofpointstointerpolate,numberofpointstointerpo
            late);
            p=pchip(x,y,xx);
            kk=1;

            %insert buffer values
            while replacestartpoint < replaceendpoint
                segmentdata(ii,replacestartpoint)=10000;
                replacestartpoint=replacestartpoint+1;
            end
        end
        jj=jj+1;
    end
    waitbar(ii / sizeofdata(1,1))
    ii=ii+1
end
close (h)
finaloutput=zeros(1,1);

ii=1

h = waitbar(0,'Please wait...');

% remove buffer values
while (ii<sizeofdata(1,1))
    jj=1;
    finaloutputjj=1;
    while (jj<sizeofdata(1,2))
        if(segmentdata(ii,jj)<10000)
            finaloutput(ii,finaloutputjj)=segmentdata(ii,jj);
            finaloutputjj=finaloutputjj+1;
        end
        jj=jj+1;
    end

    while (finaloutputjj<jj)
        finaloutputjj=finaloutputjj+1;
    end
        waitbar(ii / sizeofdata(1,1))
```

```
    ii=ii+1
end

close (h);

% write the waveform vector with error points removed.
csvwrite('correctdataremoved636465.dat',finaloutput);
```

5.4 MATLAB Grating Parameter Optimization Code

This is the code that optimizes for the physical initial parameters of the grating. This is done by calling fmincon which uses a merit function called `petersgratingopt.m`

```
close all
clear all

c=3*10^8 % define speed of light

%define swept source laser parameters
minwavelength=1534.22;
maxwavelength=1564.59;
minfreq=c/(minwavelength*10^(-9));
maxfreq=c/(maxwavelength*10^(-9));

%read in swept data files and remove errors
testa=csvread('secondtcorrectdataremoved.dat');
testa=testa(99,:);
idx=find(testa==10000);
testa=testa(1,1:idx-1);
normalize=max(testa);
normalize=normalize(1,1);
testing=testa'./normalize;

Vs = smooth (testing, 3); %Here we do a smooth instead of a DCT

sizeofdata=size(Vs');
fnew=linspace(minfreq,maxfreq,sizeofdata(1,2)); %the laser sweeps linear with
frequency and so we do a linspace
lambda=c./(fnew); %And then convert the linear frequency space into what its
wavelength equivelant should be

%plot out the first frame make sure everything looks ok, we're really only
interested in the first frame since we're optimizing for the grating
parameters.
figure(100)
plot(lambda,testing');

%now we write the data to a dat file which be read in by the merit function
dlmwrite('tester.dat', Vs, 'delimiter', ',', 'precision', 9);

Vs=testa;
cont=1;

%% find where to start for normal spectrum optimization, basically what this
does is it has 2 points start at the tip of the FBG spectrum and then move
left and right until they hit 5 percent of the maximum power of the FBG, then
we set the x position of these two points as the bounds for which we want to
optimize for the FBG parameters

idx=find(Vs==max(Vs));

idxdecrement = idx(1,1);
```

```
decrementVs=Vs(idx);

noisethreshold = 5 %this is 20 percent

while decrementVs>=(normalize/(noisethreshold))
    decrementVs=Vs(idxdecrement)
    idxdecrement = idxdecrement-1;
end

idxincrement = idx(1,1);

incrementVs=Vs(idx);

while incrementVs>=(normalize/(noisethreshold))
    incrementVs=Vs(idxincrement);
    idxincrement = idxincrement+1;
end


idxcurrent = idxdecrement;
tempmatrix = zeros(1,1);
counter = 1;
Vs=Vs';

while ( sum(tempmatrix)< sum(Vs(idxdecrement:idxincrement,1)/2))
   tempmatrix(1,counter)=Vs(idxcurrent,1);
    idxcurrent = idxcurrent+1;
    counter = counter+1;
end


% We multiply our range by 2 to make sure that we have covered the whole band
of the FBG spectrum
range = (idxincrement-idxdecrement)*2;
limits = [idxdecrement-range idxincrement+range flipboolean];
csvwrite('limits.dat',limits);

cont = 1;
Aeq=[];
Beq=[];

%the important part about using fmincon to optimize for the grating
parameters are the bounds. As long as the bounds are good, then the
optimization can turn out good results. The variables in these bounds are
dneff, the length of the grating L, the Gaussian apodization full width half
max constant in terms of mm, neff, the Bragg wavelength, and the reflectivity
lb=[0.001 5 1 1.4 1534.5 0.72];
ub=[20 14 100 1.5 1537 1];
lb=lb';
ub=ub';

%now we generate a starting point, this starting point is basically the upper
and lower bounds randomized to a certain extent
xrand=rand(1,6)
```

```
xinit=xrand';
xinit = xinit+lb;
A=[]
b=[]

%now we keep going until we have reached an acceptable threshold for
termination i.e. if cont=0, then we have reached a good threshold for
termination.
while (cont ==1)

    %this is your final array of values based on your merit function which
    %you will ahve preprogrammed in @plotta

    xfinal = fmincon(@petersgratingopt,xinit,A,b,Aeq,Beq,lb,ub);

    if(petersgratingopt(xfinal)<(0.1*1000))
        cont=0;
    else
        xrand=rand(1,6)
        xinit=xrand';
    end
end

%celebrate that the code worked well
load handel;
player = audioplayer(y, Fs);
play(player);

%write out the parameters that you're going to use for the grating.
dlmwrite('xfinaltry4.dat',xfinal, 'delimiter', ',', 'precision', 9);
```

5.5 Grating Parameter Optimization Merit Function

This is the function that is used by the grating parameters optimization code. The grating parameters are fed into this code, which generates a simulated FBG spectrum and then compares it against the measured FBG spectrum.

```
function out = petersgratingopt(x0)
%Code for calculating the reflection spectrum of a fiber Bragg grating
%using the piecewise-uniform aproach as described by Othonos and Kali

x0=x0'
tic
neff0=x0(1,4);              %Effective index of fundamental core mode
s=1;                      %Fringe visibility; set to 1 for strong gratings,
set to 0.5 for weak gratings
dneff=x0(1,1)*10^(-4);              %Change in effective index
lambda_d=x0(1,5)*10^(-9);         %Design wavelength
a0b0=[1;0];               %initial conditions 'a0' is the forward propagating
wave and 'b0' is the backward propagating wave

%Wavelength range for simulation, i.e. swept source parameters
minwavelength=1534.22;
maxwavelength=1564.59;
testagainst=csvread('tester.dat'); %read in the waveform data that we want to
optimize for
c=3*10^8;

%what is the wavelength spread that we want to zoom in on?
limits=csvread('limits.dat');
sizeofdata=size(testagainst);
minfreq=c/(minwavelength*10^(-9));
maxfreq=c/(maxwavelength*10^(-9));
fnew=linspace(minfreq,maxfreq,sizeofdata(1,1));
lambda=c./(fnew);
lambda = lambda(1,limits(1,1):limits(1,2));
testagainst=testagainst';
testagainst=testagainst(1,limits(1,1):limits(1,2));
%Period of the grating. This can either be set or calculated from the
%design wavelength
Lam=lambda_d/(2*(neff0));
%Lam=535e-9;

%Optimize for the closest 0.1 mm length
segments=round(x0(1,2));
Lengthgrating = segments*10^(-3);
segments=segments*10;
dz_temp=zeros(1,segments);
dneff_temp=zeros(1,segments);
neff_temp=zeros(1,segments);

dz_temp(1,1:segments)=0.1*10^(-3);
dneff_temp(1,1:segments)=dneff;
neff_temp(1,1:segments)=neff0;
format long
```

```
ro=x0(1,3)*10^(-3); %apodization constant i.e. Gaussian full width half max


for n=1:length(lambda)
    z=0;
    for m=1:length(dz_temp)
        dz=dz_temp(m);
        dneffk=dneff_temp(m).*exp(-(4.*log(2).*(z-
Lengthgrating/2).^2)./(ro.^2));
        pe=0.22;
        neff=neff_temp(m)+dneffk;
        zetap=2*pi/lambda(n)*(neff+dneff)-pi/(Lam*(1+(1-pe)*strain+(1-
pe)*strainchange*z));
        kappa=pi/lambda(n)*s*dneffk;              %'ac' coupling coeffiecient
        kap(n)=kappa;
        omega=sqrt(kappa.^2-zetap.^2);

        %transfer matrix kernal
       T_temp=[cosh(omega*dz)-i*zetap/omega*sinh(omega*dz)     -
i*kappa/omega*sinh(omega*dz);
                i*kappa/omega*sinh(omega*dz)
cosh(omega*dz)+i*zetap/omega*sinh(omega*dz)];
       if m==1
           T=T_temp*eye(2);
       else
           T=T_temp*T;
       end
         z=z+dz;
    end
    ambm=T*a0b0;                                %fields after propagating
through the grating
    a(n)=ambm(1);
    b(n)=ambm(2);
    r(n)=ambm(2)/ambm(1);                       %complex reflextion
coefficent
    R(n)=abs(ambm(2))^2/abs(ambm(1))^2;         %reflectance
    Tran(n)=1/abs(ambm(1))^2;                   %transmittance
    P_r(n)=R(n).*a0b0(1);                       %Power reflected
    P_t(n)=(1-R(n)).*a0b0(1);                   %Power transmitted
    P(n)=abs(10*log10(1-R(n)));                 %Power transmitted in dB
end
toc

%plot out what the error looks like
figure(1)
plot(lambda*10^9,testagainst.*x0(1,6));
hold on
plot(lambda*10^9,R,'linestyle','--');
xlabel('Wavelength (nm)');
ylabel('Reflectivity');
grid on
xlim([1536 1537])
saveas(h0, 'optimizedstructure.eps','epsc2');
out=sum(((R)-((testagainst).*x0(1,6))).^2)*1000
```

5.6 MATLAB Strain Gradient Polynomial Approximation Code

This is the code that optimizes for a strain gradient across the FBG that has the form of a second order polynomial. This is only an initial guess, since fmincon is a semi-greedy algorithm, if you fed it all the points along the grating, it would take a long time to get to the right solution based off of a correct starting point. By starting off with a second order polynomial, we limit the solution space to 3 variables. We will then use these 3 variables as a starting point later on for a point by point optimization for all the strain points along a grating. This function uses the merit function called properoptpolynomial.m included in section B6 and fmincon to optimize.

```
close all
clear all

testa=csvread('secondtcorrectdataremoved.dat'); %read in the data that needs
optimizing
testa=testa(122,:); %choose frame to optimize for
sizetesta=size(testa);

normalize=max(testa); %normalizing to make sure that we're accounting for
reflectivity
normalize=normalize(1,1);
testing=testa'./normalize;

%take discrete cosine transform in order to reduce noise
startdct=1;
enddct=1500;
x=testa(:,startdct:enddct);
X = dct(x);
[XX,ind] = sort(abs(X),'descend');
i = 1;
while norm(X(ind(1:i)))/norm(X)<0.99
   i = i + 1;
end
Needed = i;

%Reconstruct the signal and compare to the original.

X(ind(Needed+1:end)) = 0;
xx = idct(X);
Vs=[testa(1,1:startdct-1) xx testa(1,enddct-1:end)]
figure(1)
testersize=size(Vs)

%write out the testing file that you want the merit function to read in
dlmwrite('tester.dat', Vs', 'delimiter', ',', 'precision', 9);
Vs=testa;
cont=1;

%% find where to start for normal spectrum optimization. This is the same
procedure that was used in the grating parameter optimization, you start with
two points at the peak and then move down either way until you get to a
certain percentage of the power
```

```
idx=find(Vs==max(Vs));

idxdecrement = idx(1,1);
decrementVs=Vs(idx);

noisethreshold = 25 %this is 4 percent


while decrementVs>=(normalize/(noisethreshold))
    decrementVs=Vs(idxdecrement)
    idxdecrement = idxdecrement-1;
end

idxincrement = idx(1,1);

incrementVs=Vs(idx);

while incrementVs>=(normalize/(noisethreshold))
    incrementVs=Vs(idxincrement);
    idxincrement = idxincrement+1;
end

idxcurrent = idxdecrement;
tempmatrix = zeros(1,1);
counter = 1;
Vs=Vs';
while ( sum(tempmatrix)< sum(Vs(idxdecrement:idxincrement,1)/2))
   tempmatrix(1,counter)=Vs(idxcurrent,1);
    idxcurrent = idxcurrent+1;
    counter = counter+1;
end

range = round((idxincrement-idxdecrement)/2)*0;
limits = [idxdecrement-range idxincrement+range flipboolean];
csvwrite('limits.dat',limits);

cont = 1;
Aeq=[];
Beq=[];
lb=[-10000000 -10000000 0 ];
ub=[10000000 10000000 10];
lb=lb';
ub=ub';

xrand=rand(1,7)
xinit=xrand';
A=[]
b=[]

% To save time, the starting point is not random, but a guess entered by the
user of a good starting point. These are the 3 coefficients [a b c] which
relate to a*z^2+b*z++c, where z is the position along the length of the fiber
xinit = [1000 1000 2.8]
xinit = xinit'
```

```
properoptpolynomial(xinit)

% Optimize until a good solution comes out, in this case a new starting point
is not regenerated, since the starting point is generated off of user
intuition.
while (cont ==1)
    xfinal = fmincon(@properoptpolynomial,xinit,A,b,Aeq,Beq,lb,ub);
    if(properoptpolynomial(xfinal)<(1*1000))
        cont=0;
    end
end

%celebrate that a good solution was found
load handel;
player = audioplayer(y, Fs);
play(player);

%write out the answer that was optmized
dlmwrite('optimizedanswerproper122polynomialneg.dat', xfinal, 'delimiter',
',', 'precision', 9);
```

5.7 MATLAB Strain Gradient Polynomial Approximation Merit Function

This is the function that takes in the three initial variables [a,b,c] to approximate a strain gradient and generates a simulated FBG spectrum. This function then compares the simulated FBG spectrum to the measured FBG spectrum to see how close the two are. All the x0 parameters are read in from the results of grating parameter optimization.

```
function out = properoptpolynomial(x01)
%Code for calculating the reflection spectrum of a fiber Bragg grating
%using the piecewise-uniform aproach as described by Othonos and Kali, and
the modified transfer matrix method by Prabhugoud and Peters

x01=x01'
x0=csvread('xfinaltry4.dat');
x0=x0';
number=126
tic
N=2000;                    %Number of wavelength samples
M=1000;                     %Number of uniform pieces
neff0=x0(1,4);                %Effective index of fundamental core mode
s=1;                       %Fringe visliblity; set to 1 for strong gratings,
set to 0.5 for weak gratings
dneff=x0(1,1)*10^(-4);                %Change in effective index
lambda_d=x0(1,5)*10^(-9);          %Design wavelength
a0b0=[1;0];                %initial conditions 'a0' is the forward propagating
wave and 'b0' is the backward propagating wave

%Wavelength range for simulation
minwavelength=1534.22;
maxwavelength=1564.59;
testagainst=csvread('tester.dat');

c=3*10^8;
limits=csvread('limits.dat');
sizeofdata=size(testagainst);
minfreq=c/(minwavelength*10^(-9));
maxfreq=c/(maxwavelength*10^(-9));
fnew=linspace(minfreq,maxfreq,sizeofdata(1,1));
lambda=c./(fnew);
lambda = lambda(1,limits(1,1):limits(1,2));
testagainst=testagainst';
testagainst=testagainst(1,limits(1,1):limits(1,2));
%Period of the grating. This can either be set or calculated from the
%design wavelength
Lam=lambda_d/(2*(neff0));
segments=round(x0(1,2));
Lengthgrating = segments*10^(-3);
segments=segments*10;
dz_temp=zeros(1,segments);
dneff_temp=zeros(1,segments);
neff_temp=zeros(1,segments);

dz_temp(1,1:segments)=0.1*10^(-3);
```

```
dneff_temp(1,1:segments)=dneff;
neff_temp(1,1:segments)=neff0;
format long


% set terms if dealing with chirped grating, otherwise set to 0 to simulate
non chirped grating
nonlinearterminitial=0*10^(-4);
linearterminitial=0*10^(-4);
constantterminitial=0*10^(-3);

% These are parameters that would be used for a piecewise strain function
optimization as an initial guess, but in this case they're all set to 0
nonlinearterm=  0*10^(-4) ;
linearterm= 0*10^(-4);
constantterm=0*10^(-3);

%Gaussian apodization constant
ro=x0(1,3)*10^(-3);

% By assuming that the splitpoint for the piecewise function is at the origin
of the grating, the all that matters for the strain profile optimization are
the a b c coefficients that appear after the split point which leads to a
second order polynomial strain on the FBG.
splitpoint=0*10^(-3);

%Read in the strain coefficients x01
nonlineartermaftersplit=x01(1,1)*10^(-4);
linearterm aftersplit=x01(1,2)*10^(-4);
constanttermaftersplit=x01(1,3)*10^(-3);
firsttime=0;

%These matrices will hold the strain values along the FBG.
strainchangematrix=zeros(1,1);
strainchangematrixinitial=zeros(1,1);
strainmatrix=zeros(1,1);
straininitialmatrix=zeros(1,1);
z=0;

%calculate the strain points along the FBG corresponding to the 3 initial
coefficients
for ii=1:length(dz_temp)
    dz=dz_temp(ii);
    z=z+dz;
    if firsttime==0
        strainchangematrixinitial(1,ii)=0;
        strainchangematrix(1,ii)=0;
        strainmatrix(1,ii)=nonlinearterm*z^2+linearterm*z+constantterm;

straininitialmatrix(1,ii)=nonlinearterminitial*z^2+linearterminitial*z+consta
ntterminitial;
        firsttime=1;
    else
        if z>splitpoint
```

```
strainchangematrix(1,ii)=nonlineartermaftersplit*z^2+linearterm
onstanttermaftersplit-strainchangematrix(1,ii-1);

strainchangematrixinitial(1,ii)=nonlinearterminitial*z^2+linear
constantterminitial-strainchangematrixinitial(1,ii-1);

strainmatrix(1,ii)=nonlineartermaftersplit*z^2+linearterm
ttermaftersplit;

straininitialmatrix(1,ii)=nonlinearterminitial*z^2+linearterminitial*z+consta
ntterminitial;
        else

strainchangematrix(1,ii)=nonlinearterm*z^2+linearterm*z+constantterm-
strainchangematrix(1,ii-1);

strainchangematrixinitial(1,ii)=nonlinearterminitial*z^2+linearterminitial*z+
constantterminitial-strainchangematrixinitial(1,ii-1);
             strainmatrix(1,ii)=nonlinearterm*z^2+linearterm*z+constantterm;

straininitialmatrix(1,ii)=nonlinearterminitial*z^2+linearterminitial*z+consta
ntterminitial;
        end
    end
end

 % Transfer matrix calculations
for n=1:length(lambda)
    z=0;
    for m=1:length(dz_temp)
        dz=dz_temp(m);
        z=z+dz;
        dneffk=dneff_temp(m).*exp(-(4.*log(2).*(z-
Lengthgrating/2).^2)./(ro.^2));
        straininitial=straininitialmatrix(1,m);
        strain=strainmatrix(1,m);
        pe=0.22;
        strainchangeinitial=strainchangematrixinitial(1,m);
        strainchange=strainchangematrix(1,m);
        neff=neff_temp(m)+dneffk;
        zetap=2*pi/lambda(n)*(neff+dneff)-pi/((Lam*(1+(1-pe)*strain+(1-
pe)*strainchange*z))*((1+(1-pe)*straininitial+(1-
pe)*strainchangeinitial*z)));
        kappa=pi/lambda(n)*s*dneffk;             %'ac' coupling coeffiecient
        kap(n)=kappa;
        omega=sqrt(kappa.^2-zetap.^2);

        %transfer matrix kernal
        T_temp=[cosh(omega*dz)-i*zetap/omega*sinh(omega*dz)     -
i*kappa/omega*sinh(omega*dz);
              i*kappa/omega*sinh(omega*dz)
cosh(omega*dz)+i*zetap/omega*sinh(omega*dz)];
       if m==1
           T=T_temp*eye(2);
       else
```

```
            T=T_temp*T;
        end
    end
    ambm=T*a0b0;                                %fields after propagating
through the grating
    a(n)=ambm(1);
    b(n)=ambm(2);
    r(n)=ambm(2)/ambm(1);                       %complex reflextion
coefficent
    R(n)=abs(ambm(2))^2/abs(ambm(1))^2;         %reflectance
    Tran(n)=1/abs(ambm(1))^2;                   %transmittance
    P_r(n)=R(n).*a0b0(1);                       %Power reflected
    P_t(n)=(1-R(n)).*a0b0(1);                   %Power transmitted
    P(n)=abs(10*log10(1-R(n)));                 %Power transmitted in dB
end
toc

%plot out the measured vs simulated spectrum and then compare the two to see
how close they are.
Normalizationconstant=0.162500000000000; %This is the maximum value from the
original undistorted and non shifted grating spectrum

figure(1)
plot(lambda,testagainst./ Normalizationconstant.*x0(1,6),lambda,R);
out=sum(((R)-((testagainst)./ Normalizationconstant.*x0(1,6))).^2)*1000
```

5.8 MATLAB Strain Gradient Piecewise Approximation Code

This is the code that optimizes for a piecewise function as an initial guess of the strain profile along the FBG. It uses the merit function properopt and fmincon to optimize for an initial guess of the strain profile along the FBG.

```
close all
clear all

%Read in the measured waveforms
testa=csvread('secondtcorrectdataremoved.dat');

%select the waveform to optimize for
testa=testa(126,:);

% normalize spectra to account for percent reflectivity
 normalize=max(testa);
 normalize=normalize(1,1);
 testing=testa'./normalize;

%perform a DCT on the measured data to reduce noise
startdct=1;
enddct=2500;
x=testa(:,startdct:enddct);
X = dct(x);
[XX,ind] = sort(abs(X),'descend');
i = 1;
while norm(X(ind(1:i)))/norm(X)<0.98
   i = i + 1;
end
Needed = i;

%Reconstruct the signal and compare to the original.
X(ind(Needed+1:end)) = 0;
xx = idct(X);
Vs=[testa(1,1:startdct-1) xx testa(1,enddct-1:end)]
testersize=size(Vs)
dlmwrite('tester.dat', Vs', 'delimiter', ',', 'precision', 9);
Vs=testa;
cont=1;

%% find where to start for normal spectrum optimization using the 2 point
approach like in the previous optimization MATLAB files
idx=find(Vs==max(Vs));
idxdecrement = idx(1,1);
decrementVs=Vs(idx);
noisethreshold = 25 %this is 4 percent

while decrementVs>=(normalize/(noisethreshold))
decrementVs=Vs(idxdecrement)
idxdecrement = idxdecrement-1;
end

idxincrement = idx(1,1);
```

```
incrementVs=Vs(idx);

while incrementVs>=(normalize/(noisethreshold))
incrementVs=Vs(idxincrement);
idxincrement = idxincrement+1;
end

idxcurrent = idxdecrement;
tempmatrix = zeros(1,1);
counter = 1;
Vs=Vs';

while ( sum(tempmatrix)< sum(Vs(idxdecrement:idxincrement,1)/2))
tempmatrix(1,counter)=Vs(idxcurrent,1);
idxcurrent = idxcurrent+1;
counter = counter+1;
end

range = round((idxincrement-idxdecrement)/2)*0;
limits = [idxdecrement-range idxincrement+range flipboolean];
csvwrite('limits.dat',limits);

cont = 1;
Aeq=[];
Beq=[];

%these are the new bounds for the estimate on the strain profile function,
basically we break the initial estimate into 2 different polynomials along
the FBG, which yields a piecewise function. Therefore we have 6 variables to
optimize for, the variables to optimize for feed into the optimization
function following [a b c d e f g] where poly1=a*z^2+b*z+c and poly2=
d*z^2+e*z+f, and g is the point of the piecewise break given in mm
lb=[-10000000 -10000000 0 -10000000 -10000000 0 0];
ub=[10000000 10000000 10 10000000 10000000 10 10];
lb=lb';
ub=ub';
A=[]
b=[]

%to save time the user gives an initial guess using trial and error, no
random starting point will be generated if a solution fails to converge.
xinit = [0 0 9.3 0 0 0.7 3]
xinit = xinit'
properopt(xinit)

%When cont =0, that means that an acceptable solution has been found
while (cont ==1)
    xfinal = fmincon(@properopt,xinit,A,b,Aeq,Beq,lb,ub);
    if(properopt(xfinal)<(1*1000))
        cont=0;
    end
end

%celebrate the fact that a solution was found
load handel;
```

```
player = audioplayer(y, Fs);
play(player);
dlmwrite('optimizedanswerproper126piecewise.dat', xfinal, 'delimiter', ',',
'precision', 9);
```

5.9 MATLAB Strain Gradient Piecewise Approximation Merit Function

This code is the merit function for the optimization code described in B7, it takes in 2 polynomials as a piecewise function and optimizes for an initial guess on the strain function

```
function out = properopt(x01)
%Code for calculating the reflection spectrum of a fiber Bragg grating
%using the piecewise-uniform aproach as described by Othonos and Kali, and
the modified transfer matrix method by Prabhugoud and Peters modified

x01=x01'
x0=csvread('xfinaltry4.dat');
x0=x0';
number=126
tic
N=2000;                    %Number of wavelength samples
M=1000;                     %Number of uniform pieces
neff0=x0(1,4);                %Effective index of fundamental core mode
s=1;                       %Fringe visliblity; set to 1 for strong gratings,
set to 0.5 for weak gratings
dneff=x0(1,1)*10^(-4);                %Change in effective index
lambda_d=x0(1,5)*10^(-9);          %Design wavelength
a0b0=[1;0];                %initial conditions 'a0' is the forward propagating
wave and 'b0' is the backward propagating wave
%Wavelength range for simulation
minwavelength=1534.22;
maxwavelength=1564.59;
testagainst=csvread('tester.dat');

c=3*10^8;
limits=csvread('limits.dat');
sizeofdata=size(testagainst);
minfreq=c/(minwavelength*10^(-9));
maxfreq=c/(maxwavelength*10^(-9));
fnew=linspace(minfreq,maxfreq,sizeofdata(1,1));
lambda=c./(fnew);
lambda = lambda(1,limits(1,1):limits(1,2));
testagainst=testagainst';
testagainst=testagainst(1,limits(1,1):limits(1,2));
%Period of the grating. This can either be set or calculated from the
%design wavelength
Lam=lambda_d/(2*(neff0));

segments=round(x0(1,2));
Lengthgrating = segments*10^(-3);
segments=segments*10;
dz_temp=zeros(1,segments);
dneff_temp=zeros(1,segments);
neff_temp=zeros(1,segments);

dz_temp(1,1:segments)=0.1*10^(-3);
dneff_temp(1,1:segments)=dneff;
neff_temp(1,1:segments)=neff0;
format long
```

```
% set terms if dealing with chirped grating, otherwise set to 0 to simulate
non chirped grating
nonlinearterminitial=0*10^(-4);
linearterminitial=0*10^(-4);
constantterminitial=0*10^(-3);

%apodization constant
ro=x0(1,3)*10^(-3);

%terms corresponding to first polynomial before piecewise break
nonlinearterm=  x01(1,1)*10^(-4) ;
linearterm= x01(1,2)*10^(-4);
constantterm=x01(1,3)*10^(-3);

%terms corresponding to second polynomial after piecewise break
nonlineartermaftersplit=x01(1,4)*10^(-4);
lineartermaftersplit=x01(1,5)*10^(-4);
constanttermaftersplit=constantterm+x01(1,6)*10^(-3);

firsttime=0; %this is a boolean that tells the code to initialize the values
in the strain matrices to 0

%initialize the strain matrices
strainchangematrix=zeros(1,1);
strainchangematrixinitial=zeros(1,1);
strainmatrix=zeros(1,1);
straininitialmatrix=zeros(1,1);
z=0;
splitpoint=x01(1,7)*10^(-3);

for ii=1:length(dz_temp)
    dz=dz_temp(ii);
    if firsttime==0
        strainchangematrixinitial(1,ii)=0;
        strainchangematrix(1,ii)=0;
        strainmatrix(1,ii)=nonlinearterm*z^2+linearterm*z+constantterm;

straininitialmatrix(1,ii)=nonlinearterminitial*z^2+linearterminitial*z+consta
ntterminitial;
        firsttime=1;
    else
        if z>splitpoint

strainchangematrix(1,ii)=nonlineartermaftersplit*z^2+lineartermaftersplit*z+c
onstanttermaftersplit-strainchangematrix(1,ii-1);

strainchangematrixinitial(1,ii)=nonlinearterminitial*z^2+linearterminitial*z+
constantterminitial-strainchangematrixinitial(1,ii-1);

strainmatrix(1,ii)=nonlineartermaftersplit*z^2+lineartermaftersplit*z+constan
ttermaftersplit;

straininitialmatrix(1,ii)=nonlinearterminitial*z^2+linearterminitial*z+consta
ntterminitial;
        else
```

```
strainchangematrix(1,ii)=nonlinearterm*z^2+linearterm*z+constantterm-
strainchangematrix(1,ii-1);

strainchangematrixinitial(1,ii)=nonlinearterminitial*z^2+linearterminitial*z+
constantterminitial-strainchangematrixinitial(1,ii-1);
            strainmatrix(1,ii)=nonlinearterm*z^2+linearterm*z+constantterm;

straininitialmatrix(1,ii)=nonlinearterminitial*z^2+linearterminitial*z+consta
ntterminitial;
        end
    end
    z=z+dz;
end

%strain matrix calculations
for n=1:length(lambda)
    z=0;
    for m=1:length(dz_temp)
        dz=dz_temp(m);
        dneffk=dneff_temp(m).*exp(-(4.*log(2).*(z-
Lengthgrating/2).^2)./(ro.^2));
        straininitial=straininitialmatrix(1,m);
        strain=strainmatrix(1,m);
        pe=0.22;
        strainchangeinitial=strainchangematrixinitial(1,m);
        strainchange=strainchangematrix(1,m);
        neff=neff_temp(m)+dneffk;
        zetap=2*pi/lambda(n)*(neff+dneff)-pi/((Lam*(1+(1-pe)*strain+(1-
pe)*strainchange*z))*((1+(1-pe)*straininitial+(1-
pe)*strainchangeinitial*z)));
        kappa=pi/lambda(n)*s*dneffk;             %'ac' coupling coeffiecient
        kap(n)=kappa;
        omega=sqrt(kappa.^2-zetap.^2);

        %transfer matrix kernal
        T_temp=[cosh(omega*dz)-i*zetap/omega*sinh(omega*dz)     -
i*kappa/omega*sinh(omega*dz);
             i*kappa/omega*sinh(omega*dz)
cosh(omega*dz)+i*zetap/omega*sinh(omega*dz)];
        if m==1
            T=T_temp*eye(2);
        else
            T=T_temp*T;
        end
        z=z+dz;
    end
    ambm=T*a0b0;                                %fields after propagating
through the grating
    a(n)=ambm(1);
    b(n)=ambm(2);
    r(n)=ambm(2)/ambm(1);                       %complex reflextion
coefficent
    R(n)=abs(ambm(2))^2/abs(ambm(1))^2;         %reflectance
    Tran(n)=1/abs(ambm(1))^2;                   %transmittance
    P_r(n)=R(n).*a0b0(1);                       %Power reflected
```

```
    P_t(n)=(1-R(n)).*a0b0(1);                   %Power transmitted
    P(n)=abs(10*log10(1-R(n)));                 %Power transmitted in dB
end
toc

%This is the maximum value from the first undistorted FBG spectrum
normalizationconstant= 0.162500000000000

% plot out how the simulated and measured spectra look and then compare the
two to see how close they are
figure(1)
plot(lambda,testagainst./ normalizationconstant.*x0(1,6),lambda,R);
out=sum(((R)-((testagainst)./ normalizationconstant.*x0(1,6))).^2)*1000
```

5.10 MATLAB Point by Point Refine Optimization Code

This is the code that takes in the initial strain profile guess from the polynomial and piecewise approximations and refines the strain profiles by optimizing for each strain point along the grating. This is done by setting the start point as the polynomial and piecewise approximations.

```
close all
clear all

%Read in the measured FBG waveforms
testa=csvread('secondtcorrectdataremoved.dat');

%select which time frame will be optmized
testa=testa(123,:);

%normalize to take into account that reflectivity is a percentage
normalize=max(testa);
normalize=normalize(1,1);
testing=testa'./normalize;

%perform a DCT on the measurement to reduce noise
startdct=1;
enddct=1500;
x=testa(:,startdct:enddct);
X = dct(x);
[XX,ind] = sort(abs(X),'descend');
i = 1;

while norm(X(ind(1:i)))/norm(X)<0.99
   i = i + 1;
end
Needed = i;

%Reconstruct the signal and compare to the original.
X(ind(Needed+1:end)) = 0;
xx = idct(X);
Vs=[testa(1,1:startdct-1) xx testa(1,enddct-1:end)]
testersize=size(Vs)
dlmwrite('tester.dat', Vs', 'delimiter', ',', 'precision', 9);
Vs=testa;
cont=1;

%% find where to start for normal spectrum optimization using the two point
method like in previous optimization files.
idx=find(Vs==max(Vs));
idxdecrement = idx(1,1);
decrementVs=Vs(idx);
noisethreshold = 25 %this is 4 percent

while decrementVs>=(normalize/(noisethreshold))
    decrementVs=Vs(idxdecrement)
    idxdecrement = idxdecrement-1;
end
```

```
idxincrement = idx(1,1);
incrementVs=Vs(idx);

while incrementVs>=(normalize/(noisethreshold))
    incrementVs=Vs(idxincrement);
    idxincrement = idxincrement+1;
end

idxcurrent = idxdecrement;
tempmatrix = zeros(1,1);
counter = 1;
Vs=Vs';

while ( sum(tempmatrix)< sum(Vs(idxdecrement:idxincrement,1)/2))
   tempmatrix(1,counter)=Vs(idxcurrent,1);
    idxcurrent = idxcurrent+1;
    counter = counter+1;
end

range = round((idxincrement-idxdecrement)/2);
limits = [idxdecrement-range idxincrement+range flipboolean];
csvwrite('limits.dat',limits);
cont = 1;
Aeq=[];
Beq=[];

xrand=rand(1,7)
xinit=xrand';
A=[]
b=[]
answers=csvread('optimizedanswerproper123polynomialneg.dat')';
parameters=csvread('xfinaltry4.dat')';
xinit = linspace(0,round(parameters(1,2))*10^(-3),round(parameters(1,2))*10);
z=linspace(0,round(parameters(1,2))*10^(-3),round(parameters(1,2))*10);
xinit = xinit.^2*answers(1,1)*10^(-4)+xinit*answers(1,2)*10^(-
4)+answers(1,3)*10^(-3);
xinit = xinit';

%Read in the initial guess from the approximations
properoptpolynomialbitbybit(csvread('optimizedanswerproper123onebyonecorrectn
eg.dat'));

%optimize, if the optimization doesn't produce an acceptable result, then
another initial approximation must be made. The initial approximations
performed in this work have all worked very well.
while (cont ==1)
    xfinal = fmincon(@properoptpolynomialbitbybit,xinit,A,b);
    if(properoptpolynomialbitbybit(xfinal)<(1*1000))
        cont=0;
    end
end

%celebrate that a solution was found
load handel;
player = audioplayer(y, Fs);
```

```
play(player);
dlmwrite('optimizedanswerproper123onebyonecorrectneg.dat', xfinal,
'delimiter', ',', 'precision', 9);
```

5.11 Point by Point Refined Optimization Merit Function

```
function out = properoptpolynomialbitbybit(x01)
%Code for calculating the reflection spectrum of a fiber Bragg grating
%using the piecewise-uniform aproach as described by Othonos and Kali

x01=x01';
x0=csvread('xfinaltry4.dat');
x0=x0';
number=126
tic
N=2000;                    %Number of wavelength samples
M=1000;                     %Number of uniform pieces
neff0=x0(1,4);                %Effective index of fundamental core mode
s=1;                       %Fringe visliblity; set to 1 for strong gratings,
set to 0.5 for weak gratings
dneff=x0(1,1)*10^(-4);                %Change in effective index
lambda_d=x0(1,5)*10^(-9);          %Design wavelength
a0b0=[1;0];                %initial conditions 'a0' is the forward propagating
wave and 'b0' is the backward propagating wave

%Wavelength range for simulation
minwavelength=1534.22;
maxwavelength=1564.59;
testagainst=csvread('tester.dat');
c=3*10^8;
limits=csvread('limits.dat');
sizeofdata=size(testagainst);
minfreq=c/(minwavelength*10^(-9));
maxfreq=c/(maxwavelength*10^(-9));
fnew=linspace(minfreq,maxfreq,sizeofdata(1,1));
lambda=c./(fnew);
lambda = lambda(1,limits(1,1):limits(1,2));
testagainst=testagainst';
testagainst=testagainst(1,limits(1,1):limits(1,2));

%Period of the grating. This can either be set or calculated from the
%design wavelength
Lam=lambda_d/(2*(neff0));
segments=round(x0(1,2));
Lengthgrating = segments*10^(-3);
segments=segments*10;
dz_temp=zeros(1,segments);
dneff_temp=zeros(1,segments);
neff_temp=zeros(1,segments);
dz_temp(1,1:segments)=0.1*10^(-3);
dneff_temp(1,1:segments)=dneff;
neff_temp(1,1:segments)=neff0;
format long

%set all these terms t0 0 since we aren't dealing with chirped gratings or
approximations
nonlinearterminitial=0*10^(-4);
linearterminitial=0*10^(-4);
constantterminitial=0*10^(-3);
```

```
nonlinearterm=  0*10^(-4) ;
linearterm= 0*10^(-4);
constantterm=0*10^(-3);
ro=x0(1,3)*10^(-3);
firsttime=0;
strainchangematrix=zeros(1,1);
strainchangematrixinitial=zeros(1,1);
strainmatrix=zeros(1,1);
straininitialmatrix=zeros(1,1);
z=0;
splitpoint=0*10^(-3);

%populate the strain matrix and the strain change matrix with values from the
individual strain points along the FBG
for ii=1:length(dz_temp)
    dz=dz_temp(ii);
    if firsttime==0
        strainchangematrixinitial(1,ii)=0;
        strainchangematrix(1,ii)=0;
        strainmatrix(1,ii)=x01(1,ii);

straininitialmatrix(1,ii)=nonlinearterminitial*z^2+linearterminitial*z+consta
ntterminitial;
        firsttime=1;
    else
        if z>splitpoint
            strainchangematrix(1,ii)=x01(1,ii)-strainmatrix(1,ii-1);

strainchangematrixinitial(1,ii)=nonlinearterminitial*z^2+linearterminitial*z+
constantterminitial-strainchangematrixinitial(1,ii-1);
            strainmatrix(1,ii)=x01(1,ii);

straininitialmatrix(1,ii)=nonlinearterminitial*z^2+linearterminitial*z+consta
ntterminitial;
        else
           strainchangematrix(1,ii)=x01(1,ii)-strainmatrix(1,ii-1);

strainchangematrixinitial(1,ii)=nonlinearterminitial*z^2+linearterminitial*z+
constantterminitial-strainchangematrixinitial(1,ii-1);
            strainmatrix(1,ii)=x01(1,ii);

straininitialmatrix(1,ii)=nonlinearterminitial*z^2+linearterminitial*z+consta
ntterminitial;
        end
    end
    z=z+dz;
end
strainchangematrix=strainchangematrix./(0.1*10^(-3));

for n=1:length(lambda)
    z=0;
    for m=1:length(dz_temp)
        dz=dz_temp(m);
        dneffk=dneff_temp(m).*exp(-(4.*log(2).*(z-
Lengthgrating/2).^2)./(ro.^2));
        straininitial=straininitialmatrix(1,m);
```

```
        strain=strainmatrix(1,m);
        pe=0.22;
        strainchangeinitial=strainchangematrixinitial(1,m);
        strainchange=strainchangematrix(1,m);
        neff=neff_temp(m)+dneffk;
        zetap=2*pi/lambda(n)*(neff+dneff)-pi/((Lam*(1+(1-pe)*strain+(1-
pe)*strainchange*z))*((1+(1-pe)*straininitial+(1-
pe)*strainchangeinitial*z)));
        kappa=pi/lambda(n)*s*dneffk;             %'ac' coupling coeffiecient
        kap(n)=kappa;
        omega=sqrt(kappa.^2-zetap.^2);

        %transfer matrix kernal
        T_temp=[cosh(omega*dz)-i*zetap/omega*sinh(omega*dz)     -
i*kappa/omega*sinh(omega*dz);
              i*kappa/omega*sinh(omega*dz)
cosh(omega*dz)+i*zetap/omega*sinh(omega*dz)];
        if m==1
            T=T_temp*eye(2);
        else
            T=T_temp*T;
        end
        z=z+dz;
    end
    ambm=T*a0b0;                                %fields after propagating
through the grating
    a(n)=ambm(1);
    b(n)=ambm(2);
    r(n)=ambm(2)/ambm(1);                       %complex reflextion
coefficent
    R(n)=abs(ambm(2))^2/abs(ambm(1))^2;         %reflectance
    Tran(n)=1/abs(ambm(1))^2;                   %transmittance
    P_r(n)=R(n).*a0b0(1);                       %Power reflected
    P_t(n)=(1-R(n)).*a0b0(1);                   %Power transmitted
    P(n)=abs(10*log10(1-R(n)));                 %Power transmitted in dB
end
toc

%% code to save
figure(1)
plot(lambda*10^9,testagainst)
hold on
plot(lambda*10^9,R,'linestyle','--');
xlabel('Wavelength (nm)');
ylabel('Reflectivity (%)');
grid on
out=sum(((R)-((testagainst)./0.162500000000000.*x0(1,6))).^2)*1000
```